DISCLAIMER NOTICE

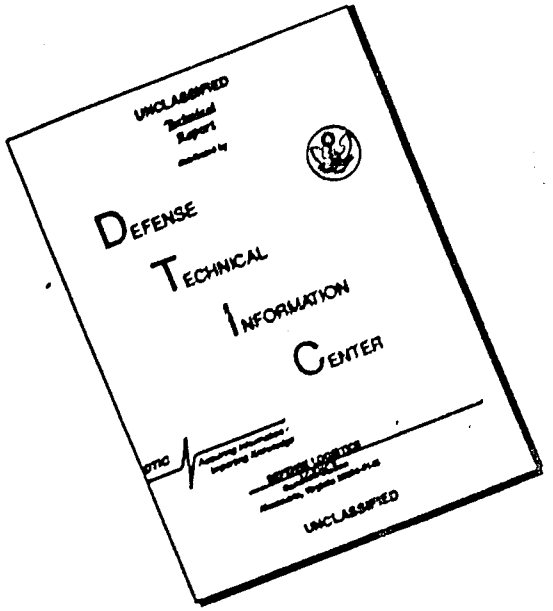

THIS DOCUMENT IS BEST QUALITY AVAILABLE. THE COPY FURNISHED TO DTIC CONTAINED A SIGNIFICANT NUMBER OF PAGES WHICH DO NOT REPRODUCE LEGIBLY.

Columbia University
in the City of New York

DEPARTMENT OF CIVIL ENGINEERING
AND ENGINEERING MECHANICS

FORCED VIBRATIONS OF A VISCO-ELASTIC CYLINDER CASE-BONDED TO A THIN ELASTIC SHELL

by

L. A. Henry and A. M. Freudenthal

Office of Naval Research
Project NR 064-446
Contract Nonr 266(78)
Technical Report No. 22

APR 8 1964

January 1964

Columbia University
in the City of New York

DEPARTMENT OF CIVIL ENGINEERING
AND ENGINEERING MECHANICS

FORCED VIBRATIONS OF A VISCO-ELASTIC CYLINDER CASE-BONDED TO A THIN ELASTIC SHELL

by

L. A. Henry and A. M. Freudenthal

Office of Naval Research
Project NR 064-446
Contract Nonr 266(78)
Technical Report No. 22

January 1964

ABSTRACT

This paper is concerned with the forced vibrations of case-bonded solid propellant grains. Special attention is paid to the interaction between the thin elastic shell (case) and the thick-walled propellant cylinder. The effects of material damping in the propellant are explored.

Frequency-response functions are computed, which can be used for analysis in situations where the loading is arbitrary deterministic or random (stationary).

TABLE OF CONTENTS

LIST OF ILLUSTRATIONS

I. INTRODUCTION

Increasing interest in the dynamic response of solid propellant rocket motors has stimulated considerable research in the area of vibrating cylinders. Many papers have been written dealing with the dynamic response of thick-walled elastic cylinders and thin cylindrical shells under various types of surface and end loads.[1-3]

The investigation presented in this paper is concerned with the vibrations of a thick-walled visco-elastic cylinder contained by and bonded to a thin cylindrical shell (Fig. 1a); the necessity for considering damping in the thick-walled cylinder is due to the fact that most solid propellants exhibit a visco-elastic response.

The solutions presented are radially-symmetric. Frequency response functions are determined which may easily be utilized for arbitrary and random inputs by means of the established methods of Harmonic Analysis.

Damping is introduced by means of the elastic-visco-elastic analogy and the use of complex moduli.[4] Poisson's ratio ν for the elastic thick-walled cylinder is replaced by $\nu^* = \nu_1 + i\nu_2$ and the shear modulus G is replaced by $G^* = G_1 + iG_2$ where $G_1 = G$ and $G_2/2\pi G_1$ denotes the specific damping $\Delta W_d/W_p$, ΔW_d being the energy dissipated during one cycle in shear and W_p the maximum shear strain energy.

Although the ratio G_2/G_1 is, generally, a function of frequency, for the present considerations it is assumed to

be constant over a relatively wide range of frequencies. This assumption of a constant complex modulus is in fair agreement with test results.[5-7]

The dependence of the damping upon the amplitude of the applied stress is neglected because its consideration would greatly complicate the equations of the problem by making them nonlinear.

The equations of linear elasticity are used for the thick-walled cylinder.[8] Membrane theory is used for the shell.[9] The equations of a higher order shell theory which includes the effects of rotatory inertia and shear are presented in Appendix A. These equations should be used in cases where membrane theory is inadequate, e.g., for external loads of acoustic nature or axial loads distributed over the ends of the shell. Appendix B gives a solution for such axial loads on the ends of the simply-supported shell which can easily be superimposed on the solution for the shell under internal pressure.

The analysis is broken down into the following steps:

1. The thick-walled cylinder
2. The thin shell.
3. The system of the thick-walled cylinder contained by and bonded to the thin shell.

The assumption that the propellant and case form a continuous structure at their interface requires continuity of displacements and therefore produces strong coupling of the motions of the cylinder and shell. This coupling is considered to be of primary importance and therefore the interaction is treated rigorously.

As a first step, a solution is obtained for a thick-walled visco-elastic cylinder with simply-supported ends and oscillating pressures on the inner and outer surfaces as well as a tangential stress on the outer surface in the axial direction.

As a second step, a solution is obtained for the thin shell with internal pressure and a tangential stress in the axial direction on the inner surface. The outer surface of the shell is traction-free.

The third step is a combination of the solutions given in steps one and two by imposing the condition that all displacements be continuous at the interface and also requiring the external loads on the cylinder to be compatible with the internal loads on the shell.

Numerical examples are given which illustrate some of the effects of varying the geometry of the structure and the specific damping in the thick-walled cylinder.

II. THE SIMPLY-SUPPORTED THICK-WALLED CYLINDER

The equation of motion of the elastic thick-walled cylinder in cylindrical coordinates is

$$G\nabla^2\underline{u} + \frac{G}{1-2\nu}\nabla\nabla\cdot\underline{u} = \rho\ddot{\underline{u}} \tag{1}$$

where

$$\nabla^2 = \frac{\partial^2}{\partial r^2} + \frac{1}{r}\frac{\partial}{\partial r} + \frac{1}{r^2}\frac{\partial^2}{\partial\theta^2} + \frac{\partial^2}{\partial z^2} \quad .$$

Application of Helmholtz's theorem to the displacement vector $\vec{u}$ allows it to be written in terms of potentials as

$$\underline{u} = \nabla\Phi + \nabla\times\underline{H} \quad . \tag{2}$$

When (2) is substituted into (1) two uncoupled wave equations on Φ and $\underline{H}$ are obtained by separation of variables

$$\begin{aligned} c_v^2\nabla^2\Phi &= \ddot{\Phi} \\ c_s^2\nabla^2\underline{H} &= \ddot{\underline{H}} \end{aligned} \tag{3}$$

where

$$c_v^2 = \frac{2G(1-\nu)}{\rho(1-2\nu)} \tag{4}$$

is the square of the velocity of propagation of dilatational waves in an infinite medium and

$$c_s^2 = \frac{G}{\rho}$$

is the square of the velocity of propagation of shear waves.

In the case of cylindrical symmetry the operator ∇^2 becomes

$$\nabla^2 = \frac{\partial^2}{\partial r^2} + \frac{1}{r}\frac{\partial}{\partial r} + \frac{\partial^2}{\partial z^2}$$

and the components of displacement are:

$$\begin{aligned} u_r &= \frac{\partial \Phi}{\partial r} - \frac{\partial H_\theta}{\partial z} \\ u_\theta &= \frac{\partial H_r}{\partial z} - \frac{\partial H_z}{\partial r} \equiv 0 \\ u_z &= \frac{\partial \Phi}{\partial z} + \frac{\partial H_\theta}{\partial r} + \frac{H_\theta}{r} \end{aligned} \tag{6}$$

The requirement that $u_\theta \equiv 0$ for the radially-symmetric case can be met by assuming $H_r = H_z = 0$, and thus the governing equations are the first of Eqs. (3) and the second with the component H_θ replacing the vector $\underline{H}$. For simplicity H_θ will now be replaced by H and the governing equations become:

$$\begin{aligned} \frac{\partial^2 \Phi}{\partial r^2} + \frac{1}{r}\frac{\partial \Phi}{\partial r} + \frac{\partial^2 \Phi}{\partial z^2} &= \frac{1}{c_v^2}\frac{\partial^2 \Phi}{\partial t^2} \\ \frac{\partial^2 H}{\partial r^2} + \frac{1}{r}\frac{\partial H}{\partial r} + \frac{\partial^2 H}{\partial z^2} &= \frac{1}{c_s^2}\frac{\partial^2 H}{\partial t^2} \end{aligned} \tag{7}$$

The displacements of interest are now:

$$u_r = \frac{\partial \Phi}{\partial r} - \frac{\partial H}{\partial z}$$

$$u_z = \frac{\partial \Phi}{\partial z} + \frac{\partial H}{\partial r} + \frac{H}{r} . \tag{8}$$

Use of these displacements results in the stress-displacement relations

$$\tau_{rr} = \frac{2G}{1-2\nu}\left[(1-\nu)\frac{\partial u_r}{\partial r} + \nu\left(\frac{u_r}{r} + \frac{\partial u_z}{\partial z}\right)\right]$$

$$\tau_{\theta\theta} = \frac{2G}{1-2\nu}\left[(1-\nu)\frac{u_r}{r} + \nu\left(\frac{\partial u_z}{\partial z} + \frac{\partial u_r}{\partial r}\right)\right]$$

$$\tau_{zz} = \frac{2G}{1-2\nu}\left[(1-\nu)\frac{\partial u_z}{\partial z} + \nu\left(\frac{\partial u_r}{\partial r} + \frac{u_r}{r}\right)\right] \tag{9}$$

$$\tau_{rz} = G\left(\frac{\partial u_r}{\partial z} + \frac{\partial u_z}{\partial r}\right) .$$

Solutions are required to satisfy the following conditions:

On the ends $z = \pm L/2$

$$\tau_{zz} = 0$$

$$u_r = 0 . \tag{10}$$

On the surface $r = a$

$$\tau_{rr} = -p_a$$

$$\tau_{rz} = 0 \tag{11}$$

and on the surface $r = b$

$$\tau_{rr} = -p_b$$
$$\tau_{rz} = t_b \ . \tag{12}$$

Solutions of Eqs. (7) are chosen of the form

$$\Phi(r,z,t) = \sum_{m=1}^{\infty} \Phi_m(r)\cos \lambda_m z \ e^{i\omega t}$$
$$H(r,z,t) = \sum_{m=1}^{\infty} H_m(r)\sin \lambda_m z \ e^{i\omega t} \ . \tag{13}$$

Substitution of Eqs. (13) into (7) gives

$$\Phi_m''(r) + \frac{1}{r}\Phi_m'(r) - k_m^2 \Phi_m(r) = 0$$
$$H_m''(r) + \frac{1}{r} H_m'(r) - h_m^2 H_m(r) = 0 \tag{14}$$

with

$$k_m^2 = \lambda_m^2 - \frac{\omega^2}{c_v^2}$$
$$h_m^2 = \lambda_m^2 - \frac{\omega^2}{c_s^2} \ . \tag{15}$$

The solutions of either of Eqs. (14) can be one of three types, depending upon whether k_m^2 or h_m^2 is negative, zero or positive. Taking the equation on Φ_m as an illustration,

(a) for $k_m^2 < 0$

$$\Phi_m = A_m J_o(k_m r) + B_m Y_o(k_m r) \tag{16}$$

(b) for $k_m^2 = 0$

$$\Phi = A \log r + B \tag{17}$$

(c) for $k_m^2 > 0$

$$\Phi_m = A_m I_o(k_m r) + B_m K_o(k_m r) \ . \tag{18}$$

In each case A_m and B_m are arbitrary constants to be determined from boundary conditions. $J_o(\alpha)$ and $Y_o(\alpha)$ are Bessel functions of the first and second kind of order zero and $I_o(\alpha)$ and $K_o(\alpha)$ are modified Bessel functions of the first and second kind of order zero and argument α .

In the following developments and computations only the range of frequencies and wave numbers for which h_m^2 and k_m^2 are real and negative has been considered.

The solutions of Eqs. (14) are therefore

$$\begin{aligned} \Phi_m(r) &= A_m J_o(k_m r) + B_m Y_o(k_m r) \\ H_m(r) &= C_m J_o(h_m r) + D_m Y_o(h_m r) \ . \end{aligned} \tag{19}$$

Equations (19) are now substituted into (8); using the recurrence relations[10]

$$J_o'(\alpha) = - J_1(\alpha) \qquad Y_o'(\alpha) = - Y_1(\alpha)$$

$$J_o''(\alpha) = \frac{1}{\alpha} J_1(\alpha) - J_o(\alpha) \qquad Y_o''(\alpha) = \frac{1}{\alpha} Y_1(\alpha) - Y_o(\alpha)$$

the expressions for the displacements are obtained

$$u_r = \sum_m \left\{ -k_m [A_m J_1(k_m r) + B_m Y_1(k_m r)] - \right.$$
$$\left. - \lambda_m [C_m J_0(h_m r) + D_m Y_0(h_m r)] \right\} \cos \lambda_m z \; e^{i\omega t}$$
$$u_z = \sum_m \left\{ -\lambda_m [A_m J_0(k_m r) + B_m Y_0(k_m r)] + \right. \tag{20}$$
$$+ C_m [\frac{1}{r} J_0(h_m r) - h_m J_1(h_m r)] +$$
$$\left. + D_m [\frac{1}{r} Y_0(h_m r) - h_m Y_1(h_m r)] \right\} \sin \lambda_m z \; e^{i\omega t} \; .$$

Substitution of Eqs. (20) into Eqs. (9) results in the expressions for the stresses

$$\tau_{rr} = \sum_m \left\{ M_1(m,r) A_m + M_2(m,r) B_m + M_3(m,r) C_m + \right.$$
$$\left. + M_4(m,r) D_m \right\} \cos \lambda_m z \; e^{i\omega t}$$
$$\tau_{rz} = \sum_m \left\{ N_1(m,r) A_m + N_2(m,r) B_m + N_3(m,r) C_m + \right. \tag{21}$$
$$\left. + N_4(m,r) D_m \right\} \sin \lambda_m z \; e^{i\omega t}$$

where

$$M_1(m,r) = 2G \left\{ [\frac{\nu-1}{1-2\nu} k_m^2 - \frac{\nu}{1-2\nu} \lambda_m^2] J_0(k_m r) + \frac{k_m}{r} J_1(k_m r) \right\}$$

$$M_2(m,r) = 2G \left\{ [\frac{\nu-1}{1-2\nu} k_m^2 - \frac{\nu}{1-2\nu} \lambda_m^2] Y_0(k_m r) + \frac{k_m}{r} Y_1(k_m r) \right\}$$

$$
\begin{aligned}
M_3(m,r) &= 2G\, h_m \lambda_m J_1(h_m r) \\
M_4(m,r) &= 2G\, h_m \lambda_m Y_1(h_m r) \\
N_1(m,r) &= 2G\, k_m \lambda_m J_1(k_m r) \\
N_2(m,r) &= 2G\, k_m \lambda_m Y_1(k_m r) \\
N_3(m,r) &= G(\lambda_m^2 - \frac{1}{r^2} - h_m^2) J_0(h_m r) \\
N_4(m,r) &= G(\lambda_m^2 - \frac{1}{r^2} - h_m^2) Y_0(h_m r) \quad .
\end{aligned} \tag{22}
$$

The loads on the surfaces of the cylinder are now assumed to be as follows:

$$
\begin{aligned}
p_a(z,t) &= P_a(z)e^{i\omega t} = \sum_m P_{am} \cos \lambda_m z\, e^{i\omega t} \\
p_b(z,t) &= P_b(z)e^{i\omega t} = \sum_m P_{bm} \cos \lambda_m z\, e^{i\omega t} \\
t_b(z,t) &= T_b(z)e^{i\omega t} = \sum_m T_{bm} \sin \lambda_m z\, e^{i\omega t}
\end{aligned} \tag{23}
$$

where

$$
\begin{aligned}
P_{am} &= \frac{2}{L} \int_{-L/2}^{L/2} P_a(z) \cos \lambda_m z\, dz \\
P_{bm} &= \frac{2}{L} \int_{-L/2}^{L/2} P_b(z) \cos \lambda_m z\, dz \\
T_{bm} &= \frac{2}{L} \int_{-L/2}^{L/2} T_b(z) \sin \lambda_m z\, dz \quad .
\end{aligned} \tag{24}
$$

The boundary conditions (11, 12) now become

$$\tau_{rr}(a,z,t) = -\sum_m P_{am} \cos \lambda_m z \, e^{i\omega t}$$

$$\tau_{rr}(b,z,t) = -\sum_m P_{bm} \cos \lambda_m z \, e^{i\omega t}$$

$$\tau_{rz}(a,z,t) = 0 \qquad (25)$$

$$\tau_{rz}(b,z,t) = \sum_m T_{bm} \sin \lambda_m z \, e^{i\omega t} \; .$$

Introduction of the above conditions (25) into Eqs. (21) results in the system of simultaneous equations shown in Table I.

TABLE I

A_m	B_m	C_m	D_m	
$M_1(m,a)$	$M_2(m,a)$	$M_3(m,a)$	$M_4(m,a)$	$-P_{am}$
$M_1(m,b)$	$M_2(m,b)$	$M_3(m,b)$	$M_4(m,b)$	$-P_{bm}$
$N_1(m,a)$	$N_2(m,a)$	$N_3(m,a)$	$N_4(m,a)$	0
$N_1(m,b)$	$N_2(m,b)$	$N_3(m,b)$	$N_4(m,b)$	T_{bm}

The solutions for A_m, B_m, C_m and D_m are as follows:

$$A_m = \frac{1}{\Delta} \begin{vmatrix} -P_{am} & M_2(m,a) & M_3(m,a) & M_4(m,a) \\ -P_{bm} & M_2(m,b) & M_3(m,b) & M_4(m,b) \\ 0 & N_2(m,a) & N_3(m,a) & N_4(m,a) \\ T_{bm} & N_2(m,b) & N_3(m,b) & N_4(m,b) \end{vmatrix}$$

$$B_m = \frac{1}{\Delta}\begin{vmatrix} M_1(m,a) & -P_{am} & M_3(m,a) & M_4(m,a) \\ M_1(m,b) & -P_{bm} & M_3(m,b) & M_4(m,b) \\ N_1(m,a) & 0 & N_3(m,a) & N_4(m,a) \\ N_1(m,b) & T_{bm} & N_3(m,b) & N_4(m,b) \end{vmatrix}$$

$$C_m = \frac{1}{\Delta}\begin{vmatrix} M_1(m,a) & M_2(m,a) & -P_{am} & M_4(m,a) \\ M_1(m,b) & M_2(m,b) & -P_{bm} & M_4(m,b) \\ N_1(m,a) & N_2(m,a) & 0 & N_4(m,a) \\ N_1(m,b) & N_2(m,b) & T_{bm} & N_4(m,b) \end{vmatrix} \qquad (26)$$

$$D_m = \frac{1}{\Delta}\begin{vmatrix} M_1(m,a) & M_2(m,a) & M_3(m,a) & -P_{am} \\ M_1(m,b) & M_2(m,b) & M_3(m,b) & -P_{bm} \\ N_1(m,a) & N_2(m,a) & N_3(m,a) & 0 \\ N_1(m,b) & N_2(m,b) & N_3(m,b) & T_{bm} \end{vmatrix}$$

with

$$\Delta = \begin{vmatrix} M_1(m,a) & M_2(m,a) & M_3(m,a) & M_4(m,a) \\ M_1(m,b) & M_2(m,b) & M_3(m,b) & M_4(m,b) \\ N_1(m,a) & N_2(m,a) & N_3(m,a) & N_4(m,a) \\ N_1(m,b) & N_2(m,b) & N_3(m,b) & N_4(m,b) \end{vmatrix} \qquad (27)$$

It is also possible to write the solutions in the form

$$\begin{aligned} A_m &= A_{m1}P_{am} + A_{m2}P_{bm} + A_{m3}T_{bm} \\ B_m &= B_{m1}P_{am} + B_{m2}P_{bm} + B_{m3}T_{bm} \\ C_m &= C_{m1}P_{am} + C_{m2}P_{bm} + C_{m3}T_{bm} \\ D_m &= D_{m1}P_{am} + D_{m2}P_{bm} + D_{m3}T_{bm} \end{aligned} \tag{28}$$

where each of the A_{mj}, B_{mj}, C_{mj} and D_{mj} $(j = 1,2,3)$ can be determined by expansion and grouping terms in Eqs. (26).

The displacements and stresses can now be written in terms of known quantities (P_{am}, P_{bm}, T_{bm}) by substitution of Eqs. (28) into (20) and then using the results in Eqs. (9). Thus the displacements are:

$$\begin{aligned} u_r = -\sum_m \Big\{ &[A_{m1}P_{am} + A_{m2}P_{bm} + A_{m3}T_{bm}]k_m J_1(k_m r) + \\ &+ [B_{m1}P_{am} + B_{m2}P_{bm} + B_{m3}T_{bm}]k_m Y_1(k_m r) + \\ &+ [C_{m1}P_{am} + C_{m2}P_{bm} + C_{m3}T_{bm}]\lambda_m J_0(h_m r) + \\ &+ [D_{m1}P_{am} + D_{m2}P_{bm} + D_{m3}T_{bm}]\lambda_m Y_0(h_m r)\Big\} \cos \lambda_m z e^{i\omega t} \end{aligned} \tag{29}$$

$$\begin{aligned} u_z = -\sum_m \Big\{ &[A_{m1}P_{am} + A_{m2}P_{bm} + A_{m3}T_{bm}]\lambda_m J_0(k_m r) + \\ &+ [B_{m1}P_{am} + B_{m2}P_{bm} + B_{m3}T_{bm}]\lambda_m Y_0(k_m r) + \\ &+ [C_{m1}P_{am} + C_{m2}P_{bm} + C_{m3}T_{bm}][h_m J_1(h_m r) - \frac{1}{r} J_0(h_m r)] + \\ &+ [D_{m1}P_{am} + D_{m2}P_{bm} + D_{m3}T_{bm}][h_m Y_1(h_m r) - \frac{1}{r} Y_0(h_m r)]\Big\} \sin \lambda_m z e^{i\omega t} \end{aligned}$$

and the stresses are

$$\tau_{rr}=\sum_m \frac{2G}{1-2\nu}\Bigg\{\Big[\Big(\nu(k_m^2-\lambda_m^2)-k_m^2\Big)J_0(k_m r)+\frac{k_m}{r}J_1(k_m r)\Big]\Big[A_{m1}P_{am}+A_{m2}P_{bm}+A_{m3}T_{bm}\Big]+$$

$$+\Big[\Big(\nu(k_m^2-\lambda_m^2)-k_m^2\Big)Y_0(k_m r)+\frac{k_m}{r}Y_1(k_m r)\Big]\Big[B_{m1}P_{am}+B_{m2}P_{bm}+B_{m3}T_{bm}\Big]+$$

$$+(1-2\nu)h_m\lambda_m\Big(J_1(h_m r)\big[C_{m1}P_{am}+C_{m2}P_{bm}+C_{m3}T_{bm}\big]+$$

$$+Y_1(h_m r)\big[D_{m1}P_{am}+D_{m2}P_{bm}+D_{m3}T_{bm}\big]\Big)\Bigg\}\cos\lambda_m z\, e^{i\omega t}$$

$$\tau_{rz}=\sum_m 2G\Bigg\{k_m\lambda_m J_1(k_m r)\big[A_{m1}P_{am}+A_{m2}P_{bm}+A_{m3}T_{bm}\big]+$$

$$+k_m\lambda_m Y_1(k_m r)\big[B_{m1}P_{am}+B_{m2}P_{bm}+B_{m3}T_{bm}\big]+$$

$$+\frac{1}{2}\Big(\lambda_m^2-\frac{1}{r^2}+h_m^2\Big)J_0(h_m r)\big[C_{m1}P_{am}+C_{m2}P_{bm}+C_{m3}T_{bm}\big]+$$

$$+\frac{1}{2}\Big(\lambda_m^2-\frac{1}{r^2}+h_m^2\Big)Y_0(h_m r)\big[D_{m1}P_{am}+D_{m2}P_{bm}+D_{m3}T_{bm}\big]\Bigg\}\sin\lambda_m z e^{i\omega t}$$

(30)

$$\tau_{\theta\theta}=-\sum_m 2G\Bigg\{\Big[\frac{k_m}{r}J_1(k_m r)+\frac{\nu}{1-2\nu}(\lambda_m^2+k_m^2)J_0(k_m r)\Big]\Big[A_{m1}P_{am}+A_{m2}P_{bm}+A_{m3}T_{bm}\Big]+$$

$$+\Big[\frac{k_m}{r}Y_1(k_m r)+\frac{\nu}{1-2\nu}(\lambda_m^2+k_m^2)Y_0(k_m r)\Big]\Big[B_{m1}P_{am}+B_{m2}P_{bm}+B_{m3}T_{bm}\Big]+$$

$$\frac{\lambda_m}{r}J_0(h_m r)\big[C_{m1}P_{am}+C_{m2}P_{bm}+C_{m3}T_{bm}\big]+$$

$$+\frac{\lambda_m}{r}Y_0(h_m r)\big[D_{m1}P_{am}+D_{m2}P_{bm}+D_{m3}T_{bm}\big]\Bigg\}\cos\lambda_m z\, e^{i\omega t}$$

$$\tau_{zz}=\sum_m 2G\Bigg\{\Big(\frac{\nu-1}{1-2\nu}\lambda_m^2-\frac{\nu}{1-2\nu}k_m^2\Big)J_0(k_m r)\big[A_{m1}P_{am}+A_{m2}P_{bm}+A_{m3}T_{bm}\big]+$$

$$+\Big(\frac{\nu-1}{1-2\nu}\lambda_m^2-\frac{\nu}{1-2\nu}k_m^2\Big)Y_0(k_m r)\big[B_{m1}P_{am}+B_{m2}P_{bm}+B_{m3}T_{bm}\big]+$$

$$+\Big[\frac{\lambda_m}{r}J_0(h_m r)-h_m\lambda_m J_1(h_m r)\Big]\big[C_{m1}P_{am}+C_{m2}P_{bm}+C_{m3}T_{bm}\big]+$$

$$+\Big[\frac{\lambda_m}{r}Y_0(h_m r)-h_m\lambda_m Y_1(h_m r)\Big]\big[D_{m1}P_{am}+D_{m2}P_{bm}+D_{m3}T_{bm}\big]\Bigg\}\cos\lambda_m z e^{i\omega t}$$

It is also observed that

$$\lambda_m = \frac{(2m-1)\pi}{L} \qquad (m = 1,2,3,\ldots)$$

is sufficient to satisfy the end conditions (Eqs. (10)).

Having the solution for the elastic thick-walled cylinder the conversion is made to the visco-elastic thick-walled cylinder by replacing the elastic shear modulus G by the complex modulus G^* and Poisson's ratio ν by a complex ν^* in the expressions for displacements and stresses.

It should be noticed here that if in Eqs. (29) and (30) the conditions $\lambda_m = 0$, $T_{bm} = 0$ and $C_m \equiv D_m \equiv 0$ are introduced the displacements and stresses become

$$u_r = [(A_1P_a + A_2P_b)J_1(kr) + (B_1P_a + B_2P_b)Y_1(kr))]e^{i\omega t} \tag{31}$$

$$u_z \equiv 0$$

and

$$\tau_{rr} = -2G\left\{[A_1P_a + A_2P_b][\frac{1-\nu}{2\nu-1}\, k\, J_o(kr) + \frac{1}{r}\, J_1(kr)] + \right.$$
$$\left. + [B_1P_a + B_2P_b][\frac{1-\nu}{2\nu-1}\, k\, Y_o(kr) + \frac{1}{r}\, Y_1(kr)]\right\} e^{i\omega t} \tag{32}$$

$$\tau_{\theta\theta} = -2G\left\{[A_1P_a + A_2P_b][\frac{\nu}{2\nu-1}\, k\, J_o(kr) - \frac{1}{r}\, J_1(kr)] + \right.$$
$$\left. + [B_1P_a + B_2P_b][\frac{\nu}{2\nu-1}\, k\, Y_o(kr) - \frac{1}{r}\, Y_1(kr)]\right\} e^{i\omega t}$$

$$\tau_{rz} \equiv 0$$

$$\tau_{zz} = -\frac{2G\nu k}{2\nu-1}\left\{[A_1P_a + A_2P_b]J_o(kr) + [B_1P_a + B_2P_b]Y_o(kr)\right\} e^{i\omega t}$$

with

$$k^2 = \omega^2/c^2 \qquad \text{and} \qquad c^2 = \frac{2(1-\nu)}{1-2\nu}\,\frac{G}{\rho}\ .$$

It can then be shown that the above stresses (32) satisfy the equation

$$\tau_{zz} = \nu(\tau_{rr} + \tau_{\theta\theta})$$

which together with the condition

$$u_z \equiv 0$$

are the requirements for a state of plane strain. Equations (31) and (32) are therefore the solution to the problem of the thick-walled cylinder in plane strain.

III. THE SIMPLY-SUPPORTED THIN CYLINDRICAL SHELL

The equations of membrane theory are used for the thin cylindrical shell.[9] For solutions which are radially symmetric the two components of displacement are w and u as shown in Fig. 1b.

The stress-displacement relations are

$$\sigma_{\theta\theta} = \frac{2\bar{G}}{1-\bar{\nu}} \left(\frac{w}{R} + \bar{\nu} \frac{\partial u}{\partial z}\right)$$
$$\sigma_{zz} = \frac{2\bar{G}}{1-\nu} \left(\bar{\nu} \frac{w}{R} + \frac{\partial u}{\partial z}\right) . \tag{33}$$

The equations of equilibrium are therefore

$$p_r - d\frac{\sigma_{\partial\theta}}{R} = M\ddot{w}$$
$$p_z + d\frac{\partial \sigma_{zz}}{\partial z} = M\ddot{u} \tag{34}$$

and by substituting Eqs. (33) into (34) the displacement equations of motion become

$$p_r - \frac{2\bar{G}d}{(1-\bar{\nu})R} \left(\frac{w}{R} + \bar{\nu} \frac{\partial u}{\partial z}\right) = M\ddot{w}$$
$$p_z + \frac{2\bar{G}d}{1-\bar{\nu}} \left(\frac{\bar{\nu}}{R} \frac{\partial w}{\partial z} + \frac{\partial^2 u}{\partial z^2}\right) = M\ddot{u} \tag{35}$$

with M the mass per unit area of the middle surface and $\bar{\nu}$ and $\bar{G}$ Poisson's ratio and the shear modulus of the shell.

It is now assumed that the external loads p_r and p_z are such that they can be represented as follows:

$$p_r = \sum_m P_{bm} \cos \lambda_m z \, e^{i\omega t}$$
$$p_z = -\sum_m T_{bm} \sin \lambda_m z \, e^{i\omega t} \tag{36}$$

with

$$\lambda_m = \frac{(2m-1)\pi}{L} \qquad (m = 1,2,3,\ldots) \, .$$

The displacements w and u are therefore taken to be of the form

$$u = \sum_m U_m \sin \lambda_m z \, e^{i\omega t}$$
$$w = \sum_m W_m \cos \lambda_m z \, e^{i\omega t} \, . \tag{37}$$

Substitution of Eqs. (36) and (37) into (35) yields the system shown in Table II.

TABLE II

U_m	W_m	
$\beta\lambda_m^2 - M\omega^2$	$\beta \frac{\bar{\nu}}{R} \lambda_m$	$-T_{bm}$
$\beta \frac{\bar{\nu}}{R} \lambda_m$	$\frac{\beta}{R^2} - M\omega^2$	P_{bm}

Solutions of the system given in Table II for U_m and W_m are the following:

$$U_m = \Delta^{-1}\left(-T_{bm}\frac{\beta}{R^2} + T_{bm}M\omega^2 - P_{bm}\frac{\beta}{R}\bar{\nu}\lambda_m\right)$$

$$W_m = \Delta^{-1}\left(P_{bm}\beta\lambda_m^2 - P_{bm}M\omega^2 + T_{bm}\frac{\beta}{R}\bar{\nu}\lambda_m\right) \tag{38}$$

with $\beta = 2d\bar{G}/1-\bar{\nu}$, d being the thickness of the shell, and Δ the determinant of the coefficients of the system given by Table II.

If quantities U_{m2}, U_{m3}, W_{m2} and W_{m3} are now appropriately defined from the coefficients of P_{bm} and T_{bm} in Eqs. (38), the displacements (Eqs. (37)) are

$$u = \sum_m (U_{m2}P_{bm} + U_{m3}T_{bm})\sin\lambda_m z\, e^{i\omega t}$$

$$w = \sum_m (W_{m2}P_{bm} + W_{m3}T_{bm})\cos\lambda_m z\, e^{i\omega t} \tag{39}$$

where P_{bm} and T_{bm} are the Fourier coefficients of the expansions for p_r and p_z as given by Eqs. (24).

The application of plane strain conditions

$$\lambda_m \equiv 0 \ , \quad T_{bm} \equiv 0$$

results in the displacements

$$u \equiv 0$$

$$w = W P_b e^{i\omega t} \tag{40}$$

where

$$W = \frac{R^2}{d(2\overline{G}/(1-\overline{\nu}) - R^2\overline{\rho}\omega^2} \quad . \tag{41}$$

It is also evident from the stresses (Eq. (33)) that

$$\sigma_{zz} = \overline{\nu}\,\sigma_{\theta\theta} \qquad (\sigma_{rr} = 0) \quad .$$

IV. THE THICK-WALLED VISCO-ELASTIC CYLINDER CASE-BONDED TO THE THIN SHELL

Section (I) contained a solution for the simply-supported thick-walled cylinder with normal pressure on its inner and outer surfaces and tangential stress on its outer surface in the axial direction. In Sec. II, a solution was given for the simply-supported shell with normal pressure and tangential stress in the axial direction on its inner surface.

These two solutions will now be combined to form a solution of the problem of the cylinder contained by the shell. The condition that displacements be continuous at the interface is expressed by the following relations:

$$\begin{aligned} u_r(b,z,t) &= w(z,t) \\ u_z(b,z,t) &= u(z,t) \ . \end{aligned} \tag{42}$$

Substitution from Eqs. (29) and (39) into (42) results in two simultaneous equations on P_{bm} and T_{bm} which allows their determination in terms of P_{am}. The equations are

$$\begin{aligned} P_{bm}\, t_2 + T_{bm}\, t_3 &= -P_{am}\, t_1 \\ P_{bm}\, \bar{t}_2 + T_{bm}\, \bar{t}_3 &= -P_{am}\, \bar{t}_1 \end{aligned} \tag{43}$$

with

$$t_j = -W_{mj} - A_{mj}k_m J_1(k_m b) - B_{mj}k_m Y_1(k_m b) -$$

$$- C_{mj}\lambda_m J_0(h_m b) - D_{mj}\lambda_m Y_0(h_m b)$$

$$\bar{t}_j = -U_{mj} - A_{mj}\lambda_m J_0(k_m b) - B_{mj}\lambda_m Y_0(k_m b) -$$

$$- C_{mj}[h_m J_1(h_m b) - \tfrac{1}{b}J_0(h_m b)] - D_{mj}[h_m Y_1(h_m b) - \tfrac{1}{b}Y_0(h_m b)]$$

for $j = 1,2,3$ and in each case

$$U_{m1} = W_{m1} = 0 \ . \tag{45}$$

The solutions of (43) are therefore

$$\bar{P}_{bm} = \frac{P_{bm}}{P_{am}} = \frac{\bar{t}_1 t_3 - t_1 \bar{t}_3}{t_2 \bar{t}_3 - \bar{t}_2 t_3}$$

$$\bar{T}_{bm} = \frac{T_{bm}}{P_{am}} = \frac{\bar{t}_2 t_1 - t_2 \bar{t}_1}{t_2 \bar{t}_3 - \bar{t}_2 t_3} \ . \tag{46}$$

Substituting (46) into (39) gives the displacements of the shell in terms of known quantities

$$u = \sum_m P_{am}(U_{m2}\bar{P}_{bm} + U_{m3}\bar{T}_{bm})\sin \lambda_m z \ e^{i\omega t}$$

$$w = \sum_m P_{am}(W_{m2}\bar{P}_{bm} + W_{m3}\bar{T}_{bm})\cos \lambda_m z \ e^{i\omega t} \ . \tag{47}$$

A similar substitution into Eqs. (29) and (30) can be made for the displacements and stresses in the thick-walled cylinder.

The ratio P_b/P_a for plane strain is found, either by applying the first Eq. (42) to satisfy continuity of displacement using (31) and (40), or by imposing the conditions

$$\lambda_m = 0 \ , \quad C_m = 0 \ , \quad D_m = 0$$

on the first Eq. (46).

The result is

$$P_b/P_a = \frac{(1-\nu)k}{D} \left[J_o(kb)Y_1(kb) - Y_o(kb)J_1(kb) \right] \tag{48}$$

where

$$\begin{aligned} D = {} & \left[(1-\nu)k\, J_o(ka) + (2\nu-1)\frac{1}{a} J_1(ka) \right] Y_1(kb) - \\ & - \left[(1-\nu)k\, Y_o(ka) + (2\nu-1)\frac{1}{a} Y_1(ka) \right] J_1(kb) - \\ & - \frac{2R^2 G\Delta}{(2\nu-1)d\left[2\bar{G}/(1-\bar{\nu}) - R^2\bar{\rho}\omega^2\right]} \end{aligned} \tag{49}$$

with

$$\begin{aligned} \Delta = {} & \left[(1-\nu)kJ_o(ka) + (2\nu-1)\frac{1}{a}J_1(ka) \right] \left[(1-\nu)kY_o(kb) + (2\nu-1)\frac{1}{b}Y_1(kb) \right] - \\ & - \left[(1-\nu)kJ_o(kb) + (2\nu-1)\frac{1}{b}J_1(kb) \right] \left[(1-\nu)kY_o(ka) + (2\nu-1)\frac{1}{a}Y_1(ka) \right] \end{aligned} \tag{50}$$

V. NUMERICAL EXAMPLES

In order to illustrate the results of the analysis in the previous sections, certain numerical calculations were carried out. It was assumed that the internal pressure in the thick-walled cylinder was of the form $P_a e^{i\omega t}$ with P_a constant. This latter assumption is, of course, an approximation, since it is known that a well defined smooth burning surface would not exist even in a solid fuel rocket motor which initially had a circular bore.[11] Therefore the transition region where the burning takes place is not being considered. The overall effect on the remainder of the propellant is assumed to be taken care of by an equivalent pressure distribution. The effect on the analysis of the moving internal boundary is also neglected. However, a step by step increase of the ratio a/b is felt to be a reasonable approximation of this moving boundary.

Computations were made for the circumferential stress $\tau_{\theta\theta}$ at $z = 0$ on the inner surface ($r = a$) of the thick-walled cylinder and at the interface ($r = b$) for certain combinations of parameters. At $r = b$ the quantities τ_{rr}, τ_{rz} and u_r were also computed for one combination of parameters.

For the numerical calculations, the following dimensionless parameters were fixed:

1) The ratio of the length to the outer radius of the thick-walled cylinder ($L/b = 5.0$) .

2) The ratio of the shear modulus of the shell to that of the cylinder ($\bar{G}/G = 10^4$) .

3) Poisson's ratio for the thick-walled cylinder ($\nu = .4$) .

4) Poisson's ratio for the shell ($\bar{\nu} = .3$) .

5) The ratio of the mass density of the cylinder to that of the shell ($\rho/\bar{\rho} = .5$) .

Certain other parameters were varied as indicated below.

1) The ratio of the inner to the outer radius of the thick-walled cylinder was given the values

$$a/b = .25, .5, .75, .95$$

2) The ratio of the outer radius of the thick-walled cylinder to the thickness of the shell was given values

$$b/d = 500, 750, 1000$$

3) The specific damping in the cylinder was varied by allowing the ratio of the imaginary to the real part of the complex modulus to assume the values

$$G_2/G_1 = .1, .2, .3 .$$

Each diagram illustrates the frequency dependence of the quantity which is plotted. The independent variable in each case is a dimensionless frequency defined by the equation

$$\bar{\omega} = 10^5 \frac{\omega d}{2\pi} \sqrt{\frac{\bar{\rho}}{G}} .$$

All calculations were done on the IBM 7090 Date processing system.

VI. DISCUSSION AND CONCLUSIONS

All computations were made for $m = 1$ i.e., for the first barrelling mode of the structure. This is associated with the first term of the expansion for the internal pressure. Figure 2 shows a comparison of this $(m = 1)$ term with a sum of the series and it appears that this first term is a good approximation for the behavior as a whole in the considered range.

An independent computation of the natural frequencies of the thick-walled cylinder shows that in the range under consideration there are fewer roots of the frequency equation than there are natural frequencies of the combined structure of the cylinder and shell Fig.7a. In each case the first natural frequency of the shell in this mode is beyond the range of interest. It is therefore evident that additional resonant frequencies are encountered in the range of interest because of the coupling of the motions of the cylinder and shell. Figures 3a and 8a indicate this increase in the number of natural frequencies. Figure 3b illustrates the effects of very small damping $(G_2/G_1 = .001)$ on the circumferential stress at the bore for $a/b = .5$, $b/d = 1000$, $L/b = 5.0$. It can be seen that all the resonant peaks are still clearly defined. Figure 3c indicates the effects of higher damping $(G_2/G_1 = .1, .2,$ and $.3)$ on the same stress for the same geometry. Here it is clear that some of the resonant peaks have already been completely damped out for the value $G_2/G_1 = .1$. It seems apparent therefore that since the cylinder is in its first breathing mode, the resonant peaks

which are so easily damped out must be associated with secondary shearing effects that are coupled with the barrelling motion. For higher values of damping (G_2/G_1 = .2 and .3) there still remains at leastone prominent resonant peak. This is associated with the first resonant frequency of the breathing mode of the structure.

Figures 7 to 16a,b,c illustrate the effect of changing geometry on the response in the range of interest. It is clear that as a b · 1 (Figs. 3c, 7b, 8b, 9b) the dominant resonant frequency shifts towards a value which is the first resonant frequency of the shell by itself. As the change takes place, i.e., as the visco-elastic cylinder gets relatively thinner it is also clear that the amplitude of the response at the resonant frequency increases in magnitude tending towards the limiting case of the infinite value which would be associated with the elastic shell at its natural frequency. A similar shifting of the frequencies can be observed as b/d varies from 1000 to 500 Figs. 7b, 10b, 14b). This amounts to a relative thickening of the shell. In this case however, the effects of damping do not disappear as fast, since in this case, the relative thickness of the cylinder is held constant while the shell is made thicker. A study of Fig. 7 to 16b would therefore indicate that there is a certain set of ratios a/b and b/d for which the maximum effect of the damping in the thick-walled cylinder would be achieved.

Figures 3d and 7 to 16c illustrate the effects of damping on the circumferential stress at the interface (r = b). It is clearly noticeable that in certain cases (Figs. 3d, 10c and 14c) where the cylinder is still much thicker than the shell, the amplitude of the stress at the interface is

very much smaller than at the bore even though the resonant peaks are still evident. However, as is seen in Figs. 9c, 12c and 16c as $a/b \to 1$ the amplitude again becomes very large as the resonant frequency approaches that of the elastic shell by itself.

Figures 4a,b and 8a,b show one case of the radial stress and displacement at the interface for $z = 0$, while Fig. 5a,b shows the shear stress at the interface for $z = \pm L/2$. As would be expected for this mode the shear stress is much smaller in amplitude than the circumferential or radial stresses. However, it is interesting to note that in this case there is still evidence of all the peaks for $G_2/G_1 = .1$ whereas for the other stresses most of these have already been completely damped out. Therefore, there seems to be evidence here to support the earlier conclusion that those peaks in the other stresses which disappeared for very low damping were due to frequencies associated with shearing.

It is apparent from the results discussed above that values of $G_2/G_1 = .1, .2, .3$ have a drastic effect upon the amplitudes of the frequency response functions which were computed. Since these values are smaller than values measured experimentally $(G_2/G_1 = .35)$[12] it seems reasonable to conclude that any analysis of a solid fuel rocket motor which does not take into consideration the visco-elastic effects of the propellant would not give a true overall picture.

The variation of the ratio a/b, as a simulation of the state of the structure at various stages of burning, indicates for certain ranges of frequency, a considerable increase in the amplitudes of the computed functions. This implies that, in fact, in a structure of this type, the critical period would be in the later stages when the pro-

pellant is almost completely burnt out. From this point of view, the important frequency might be close to the first breathing frequency of the thin shell.

However, the diagrams indicate that for certain restricted ranges of the forcing frequency a judicious choice of parameters may be enough to eliminate the possibility of large amplitude resonant peaks.

APPENDIX A

HIGHER ORDER SHELL THEORY

In cases of dimensions and loads for which membrane theory is inadequate, a higher order theory is required. The theory presented here includes the effects of rotatory inertia and shear.[13]

For the radially symmetric case the displacements are

$$\begin{aligned} u_r(x,z,t) &= w(z,t) \\ u_z(x,z,t) &= u(z,t) + x\psi(z,t) \end{aligned} \tag{A1}$$

with u, w, as shown in Fig. 1b, $x = r-R$ and ψ the angle of rotation of fibers which in the initial state are perpendicular to the middle surface.

The relevant strains are

$$\begin{aligned} \epsilon_{\theta\theta} &= \frac{u_r}{R} \\ \epsilon_{zz} &= \frac{\partial u_z}{\partial z} \\ \epsilon_{rz} &= \frac{1}{2}\left(\frac{\partial u_z}{\partial x} + \frac{\partial u_r}{\partial z}\right) . \end{aligned} \tag{A2}$$

Although unrestricted Poisson's ratio effect is allowed in the radial direction and at the same time the displacements seem to imply $\epsilon_{rr} = 0$, the contradiction can be removed by first eliminating ϵ_{rr} from the stress-strain relations.

Thus

$$\sigma_{\theta\theta} = \frac{\nu}{1-\nu}\sigma_{rr} + \frac{2G}{1-\nu}\epsilon_{\theta\theta} + \frac{2G\nu}{1-\nu}\epsilon_{zz}$$

$$\sigma_{zz} = \frac{\nu}{1-\nu}\sigma_{rr} + \frac{2G\nu}{1-\nu}\epsilon_{\theta\theta} + \frac{2G}{1-\nu}\epsilon_{zz} \qquad (A3)$$

$$\sigma_{rz} = 2G\epsilon_{rz} \ .$$

If σ_{rr} is now considered to be zero the stresses are

$$\sigma_{\theta\theta} = \frac{2G}{1-\nu}\left\{\frac{w}{R} + \nu\left(\frac{\partial u}{\partial z} + x\frac{\partial \psi}{\partial z}\right)\right.$$

$$\sigma_{zz} = \frac{2G}{1-\nu}\left\{\frac{\partial u}{\partial z} + x\frac{\partial \psi}{\partial z} + \nu\frac{w}{R}\right\} \qquad (A4)$$

$$\sigma_{rz} = K^2G\left(\psi + \frac{\partial w}{\partial z}\right)$$

where K^2 is a constant as used in Mindlin's plate theory to adjust the limiting velocity for short waves to that given by three-dimensional theory.[14]

Integration of the above stresses through the thickness of the shell gives forces and moments in terms of displacements as

$$N_z = \beta\left[\frac{\partial u}{\partial z} + \nu\frac{w}{R}\right]$$

$$N_\theta = \beta\left[\frac{w}{R} + \nu\frac{\partial u}{\partial z}\right] \qquad (A5)$$

$$M_z = \delta\frac{\partial \psi}{\partial z}$$

$$M_\theta = \nu\delta\frac{\partial \psi}{\partial z}$$

$$Q_z = \kappa(\psi + \frac{\partial w}{\partial z}) \tag{A5}$$

with

$$\beta = \frac{2dG}{1-\nu} \; ; \quad \delta = \frac{d^3G}{6(1-\nu)} \; ; \quad \kappa = K^2 dG \; .$$

All other forces and moments are zero. Application of the necessary conditions for equilibrium of a section of the shell results in three uncoupled equations on u, w, and ψ

$$\beta(R\frac{\partial^2 u}{\partial z^2} + \nu\frac{\partial w}{\partial z}) + R\,p_z - RM\ddot{u} = 0$$

$$\beta(\frac{w}{R} + \nu\frac{\partial u}{\partial z}) - \kappa(R\frac{\partial \psi}{\partial z} + R\frac{\partial^2 w}{\partial z^2}) - R\,p_x + RM\ddot{w} = 0 \tag{A6}$$

$$\delta R\frac{\partial^2 \psi}{\partial z^2} - \gamma(R\psi + R\frac{\partial w}{\partial z}) - R\frac{d}{2}p_z - RI\ddot{\psi} = 0$$

where M is the mass and I the moment of Inertia per unit area of the middle surface of the shell.

It can be shown that a unique solution of the system (A6) can be obtained if one quantity of each of the pairs $N_z u$, $M_z \psi$ and $Q_z w$ is prescribed on boundaries z = constant.

It can also be shown that Eqs. (35) can be obtained very easily from (A6) by letting $\psi = -\partial w/\partial z$ and neglecting rotatory inertia ($I = 0$) and bending rigidity ($\delta = 0$). If the loading is the same as given by (36) in Sec. II, the solution procedure is analogous, the only difference being that in the case of the higher order theory, the expressions for $\overline{t}_j$ in (44) will contain an additional term due to ψ .

Numerical calculations were made using the higher order theory in this section for the same range as for the simple shell theory, and it was found that in this range, the results were identical. This agrees with the results of Greenspon.[15]

APPENDIX B

SOLUTIONS OF HIGHER ORDER SHELL EQUATIONS FOR LONGITUDINAL LOADS DISTRIBUTED OVER THE ENDS

Solutions to Eqs. (A6) are taken of the form

$$u = Ue^{i(\lambda z+\omega t)}$$

$$w = We^{i(\lambda z+\omega t)} \qquad \text{(B1)}$$

$$\psi = \Psi e^{i(\lambda z+\omega t)} \quad .$$

Substitution of Eqs. (B1) into Eqs. (A6) gives a system of equations on U, W and Ψ which is homogeneous ($p_x = 0$, $p_z = 0$) as shown in Table B-I.

TABLE B-I

U	W	Ψ	
$-\beta\lambda^2 + M\omega^2$	$\frac{\beta}{R}\nu i\lambda$	0	0
$\frac{\beta}{R}\nu i\lambda$	$\frac{\beta}{R^2} + \gamma\lambda^2 - M\omega^2$	$-\gamma i\lambda$	0
0	$-\gamma i\lambda$	$-\delta\lambda^2 - \gamma + I\omega^2$	0

In order to have a non-trivial solution of the system given in Table B-I, the requirement is that the determinant of the coefficients of U, W and Ψ be equal to zero. This expanded determinant is the frequency-wavelength relationship for the shell.

If a dimensionless wavenumber $\bar{\lambda} = d/\lambda$ is defined it can be shown that there are three limiting values of the frequency $\bar{\omega}$ as this wavelength approaches zero. These values are determined by the roots of the equation:

$$\bar{\omega}^6 - \left(\frac{3}{\pi^2} + \frac{\bar{d}^2}{2\pi^2(1-\nu)}\right)\bar{\omega}^4 + \frac{3\bar{d}^2}{2\pi^4(1-\nu)}\bar{\omega}^2 = 0 \qquad (B2)$$

with

$$\bar{d}^2 = d^2/R^2 \qquad \text{and} \qquad \bar{\omega}^2 = \frac{\omega^2 d^2 \rho}{4\pi^2 G} \quad .$$

The roots in ascending order of magnitude are

$$\bar{\omega}_1^2 = 0 \; ; \quad \bar{\omega}_2^2 = \frac{\bar{d}^2}{2\pi^2(1-\nu)} \; ; \quad \bar{\omega}_3^2 = \frac{3}{\pi^2} \quad . \qquad (B3)$$

The first root ($\bar{\omega}_1^2 = 0$) corresponds to a rigid body displacement of the shell in the axial direction. The remainder of the branch which passes through this point gives frequency-wavelength relations for purely axial motions (extensions) of the middle surface of the shell.

The second root ($\bar{\omega}_2^2 = \bar{d}^2/2\pi^2(1-\nu)$) corresponds to the lowest "breathing" mode of the shell. The motion in this mode can be compared to the vibrations of a circular ring in its plane.[16]

The equation for the actual frequency is in this case

$$\omega_2^2 = \frac{2(1+\nu)G}{R^2(1-\nu^2)} = \frac{\omega_T^2}{1-\nu^2} \qquad (B4)$$

where ω_T refers to Timoshenko's value for the frequency of the lowest mode of a vibrating ring.[15] The factor $(1-\nu^2)$ appearing in the denominator is a correction which is due to the effect of the adjacent rings of the shell upon each other.

It should also be noted that $\lim_{R \to \infty} \omega_2^2 = 0$ indicating that this mode could not exist in a plate.

The third root $(\overline{\omega}_3^2 = 3/\pi^2)$ corresponds to the cut-off frequency for axial shear in the shell.

The expansion of the determinant given in Table B-I, has three roots λ^2 which are frequency dependent.

In the range where these are real, the solutions (B-I) become

$$u = \sum_{k=1}^{3} U_k \, e^{i(\pm\lambda_k(\omega)z+\omega t)}$$

$$w = \sum_{k=1}^{3} W_k \, e^{i(\pm\lambda_k(\omega)z+\omega t)} \qquad (35)$$

$$\psi = \sum_{k=1}^{3} \Psi_k \, e^{i(\pm\lambda_k(\omega)z+\omega t)} \; .$$

It is also possible to determine ratios

$$\frac{U_k}{W_k} = \frac{\beta\nu i\lambda_k(\omega)}{R\beta\lambda_k^2(\omega) - RM\omega^2}$$

$$\frac{\Psi_k}{W_k} = \frac{\gamma i \lambda_k(\omega)}{I\omega^2 - \gamma - \delta \lambda_k^2(\omega)} \quad . \tag{B6}$$

Symmetric portions (symmetry with respect to $z = 0$) of the solution are therefore

$$u = \sum_{k=1}^{3} \frac{\beta\nu}{R} \frac{\lambda_k(\omega) W_k \sin \lambda_k(\omega) z}{M\omega^2 - \beta \lambda_k^2(\omega)} e^{i\omega t}$$

$$w = \sum_{k=1}^{3} W_k \cos \lambda_k(\omega) e^{i\omega t} \tag{B7}$$

$$\psi = \sum_{k=1}^{3} \frac{\gamma \lambda_k(\omega) W_k \sin \lambda_k(\omega) z}{\gamma - I\omega^2 - \delta \lambda_k^2(\omega)} e^{i\omega t} \quad .$$

Using these latter equations it is now possible to determine eigenfunctions and natural frequencies for symmetric motions, by imposing the necessary boundary conditions.

Using Eqs. (B7) above and Eqs. (A5) the following boundary conditions are applied:

$$\left.\begin{aligned} w &= 0 \\ M_z &= 0 \\ N_z &= N e^{i\omega t} \end{aligned}\right\} z = \pm L/2 \tag{B8}$$

Substitution of Eqs. (B7) into (B8) results in the system shown in Table B-II.

TABLE B-II

W_1	W_2	W_3	
$\cos \lambda_1 L/2$	$\cos \lambda_2 L/2$	$\cos \lambda_3 L/2$	0
$\dfrac{\gamma\lambda_1^2 \cos \lambda_1 L/2}{I\omega^2 - \gamma - \delta\lambda_1^2}$	$\dfrac{\gamma\lambda_2^2 \cos \lambda_2 L/2}{I\omega^2 - \gamma - \delta\lambda_2^2}$	$\dfrac{\gamma\lambda_3^2 \cos \lambda_3 L/2}{I\omega^2 - \gamma - \delta\lambda_2^2}$	0
$\dfrac{\beta\nu M\omega^2 \cos \lambda_1 L/2}{R(M\omega^2 - \beta\lambda_1^2)}$	$\dfrac{\beta\nu M\omega^2 \cos \lambda_2 L/2}{R(M\omega^2 - \beta\lambda_2^2)}$	$\dfrac{\beta\nu M\omega^2 \cos \lambda_3 L/2}{R(M\omega^2 - \beta\lambda_3^2)}$	N

This system can now be solved for W_k $(k = 1,2,3)$ in terms of N the amplitude of the applied load as follows:

$$W_1 = \frac{N}{\Delta}\left\{\frac{\gamma\lambda_3^2}{\gamma - I\omega^2 + \delta\lambda_2^2} - \frac{\gamma\lambda_3^2}{\gamma - I\omega^2 + \delta\lambda_3^2}\right\}\cos \lambda_2 L/2 \cos \lambda_3 L/2$$

$$W_2 = \frac{N}{\Delta}\left\{\frac{\gamma\lambda_3^2}{\gamma - I\omega^2 + \delta\lambda_3^2} - \frac{\gamma\lambda_1^2}{\gamma - I\omega^2 + \delta\lambda_1^2}\right\}\cos \lambda_3 L/2 \cos \lambda_1 L/2 \quad (B9)$$

$$W_3 = \frac{N}{\Delta}\left\{\frac{\gamma\lambda_1^2}{\gamma - I\omega^2 + \delta\lambda_1^2} - \frac{\gamma\lambda_2^2}{\gamma - I\omega^2 + \delta\lambda_2^2}\right\}\cos \lambda_1 L/2 \cos \lambda_2 L/2 \ .$$

These quantities can then be substituted into Eqs. (B7) and then combined by Eqs. (A1) to give the displacements in the shell as

$$u_r = \sum_{k=1}^{3} W_k \cos \lambda_k(\omega) z \, e^{i\omega t}$$

$$u_z = \sum_{k=1}^{3} \left\{ \left[\frac{\beta\nu}{R(M\omega^2 - \beta \lambda_k^2(\omega))} + \frac{x\gamma}{\gamma - I\omega^2 + \delta\lambda_k^2(\omega)} \right] \lambda_k(\omega) W_k \sin \lambda_k(\omega) z \right\} e^{i\omega t} \quad . \tag{B10}$$

Since the problem is linear, the results above can be superimposed upon those given in Sec. II to be used as a solution for the combined loading of internal pressure on the thick-walled cylinder and longitudinal loads on the ends of the shell.

The super-position could be carried out by first expanding the results (B10) into Fourier Series and then combining the results with the series given by Eqs. (39).

BIBLIOGRAPHY

1. J. A. McFadden, "Radial Vibrations of Thick-Walled Hollow Cylinders," J. Acoustical Soc. Am., 26, 714-715 (1956).

2. J. F. Bird, R. W. Hart and F. T. McClure, "Vibrations of Thick-Walled Hollow Cylinders: Exact Numerical Solutions," J. Acoustical Soc. Am., 32:11 (November, 1960).

3. J. H. Baltrukonis, M. Chi and W. G. Gottenberg, Free Transverse Vibrations in an Infinitely-Long Layered Elastic Cylinder, Technical Report No. 3, NASA Research Grant No. NsG-125-61 (Suppl. 1-62) (August, 1952).

4. A. M. Freudenthal and H. Geiringer, "The Mathematical Theories of the Inelastic Continuum," Vol. VI: Encyclopedia of Physics, Berlin: Springer-Verlag, 1958.

5. W. Philippoff, "Mechanical Investigation of Elastomers in a Wide Range of Frequencies," J. Appl. Physics, 24, 685 (1953).

6. L. J. Zopas, S. L. Shufler, and T. W. DeWitt, "A Comparison of the Dynamic Properties of Natural Rubber and GR-S," J. Polymer Science, 18, 245 (1955).

7. J. D. Ferry, "Structure and Mechanical Properties of Plastics," Bd. IV: Die Physik der Hochpolymeren, H. A. Stuart (ed.), Berlin: Springer-Verlag, 1956.

8. A. E. H. Love, A Treatise on the Mathematical Theory of Elasticity, 4th ed. (1927), New York: Dover Publications, Inc., 1944.

9. M. L. Baron and H. H. Bleich, Tables for Frequencies and Modes of Free Vibration of Infinitely Long Thin Cylindrical Shells, ASME Paper No. 53 - A-33.

10. E. T. Whittaker and G. N. Watson, A Course in Modern Analysis, 4th ed. (1927), Cambridge: Cambridge University Press, 1944.

11. Martin Summerfield (ed.), "Solid Propellant Rocket Research," Vol. I: Progress in Astronautics and Rocketry, New York: Academic Press, 1960.

12. Atlantic Research Corp., "Dynamic Mechanical Properties of Solid Propellants," ARPA No. 22-61 Project Code No. 009-06-001 Contract No. NOw 61-1054-C, Quarterly Technical Summary Report, December 31, 1962.

13. I. Mirsky and G. Herrmann, "Three-Dimensional and Shell-Theory Analysis of Axially-Symmetric Motions of Cylinders," Journal of Applied Mechanics, Trans. ASME, Vol. 78 563-568 (December 1956).

14. R. D. Mindlin, "Influence of Rotatory Inertia and Shear on Flexural Vibrations of Isotropic, Elastic Plates," J. Appl. Mech., 18, Trans. ASME, 73, 31-38 (1951).

15. J. E. Greenspon, "Vibrations of a Thick-Walled Cylindrical Shell.Comparison of the Exact Theory with Approximate Theories," J. Acoust. Soc. Am., 32, 571-578 (1959).

16. S. Timoshenko, Vibration Problems in Engineering, 3rd ed., New York: Van Nostrand, 1955.

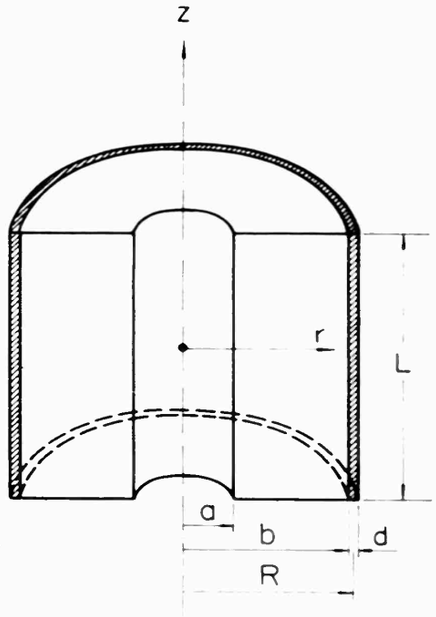

Figure 1a

Section of Thick-Walled Cylinder and Shell Showing Dimensions and Coordinates

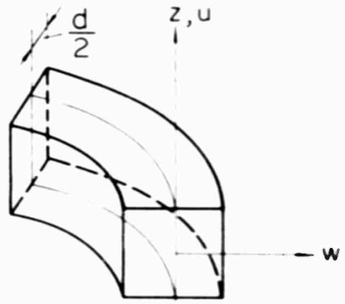

Figure 1b

Section of Shell Showing Coordinates

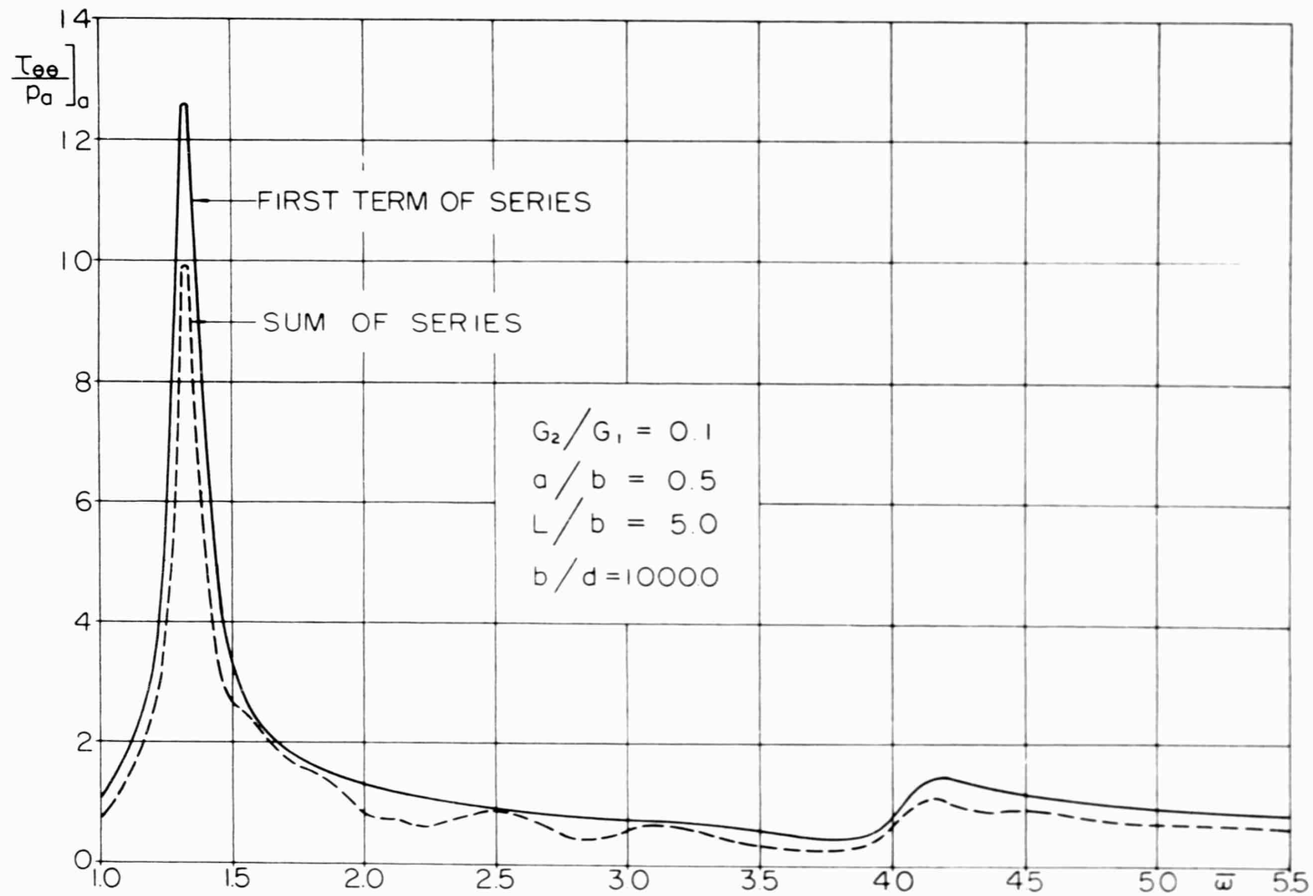

Figure 2 Absolute Value of Circumferential Stress at the Bore Showing Comparison Between the First Term and the Sum of the Series ($a/b = .5$, $b/d = 1000$)

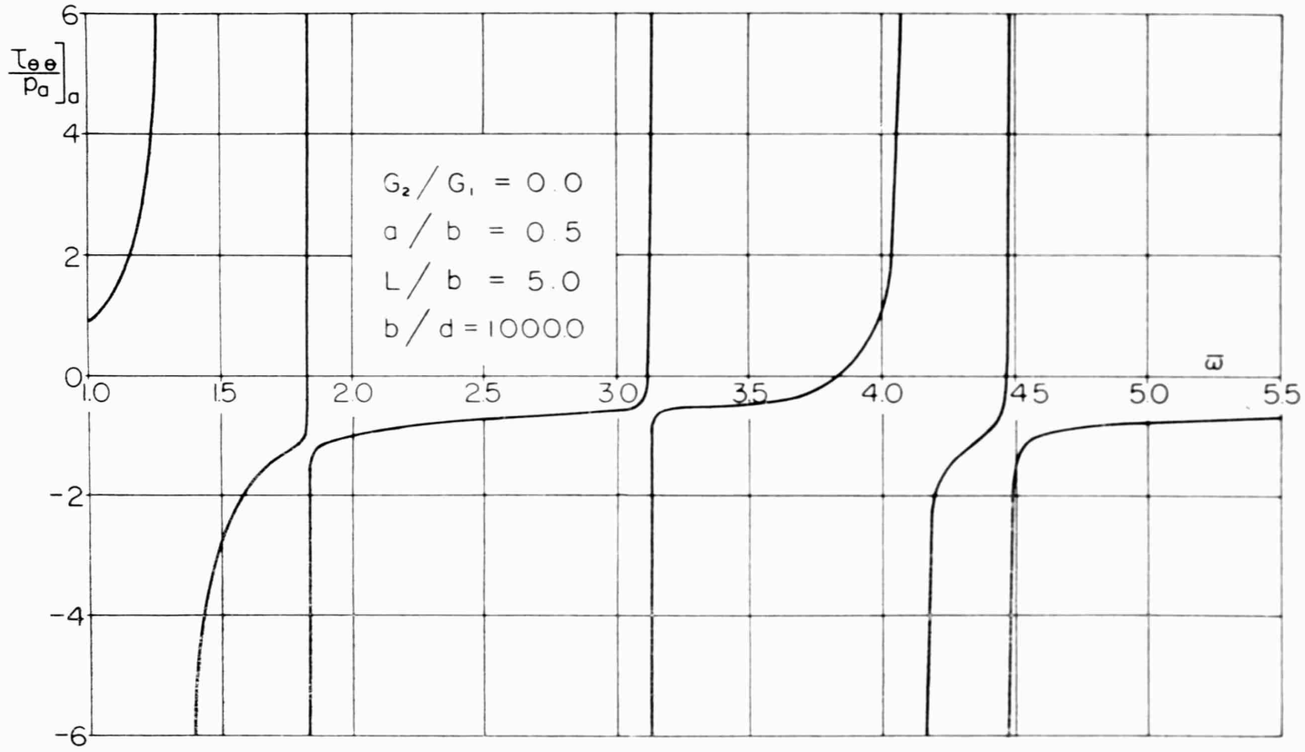

Figure 3a Circumferential Stress at the Bore for the Elastic Cylinder and Shell (a/b = .5 , b/d = 1000)

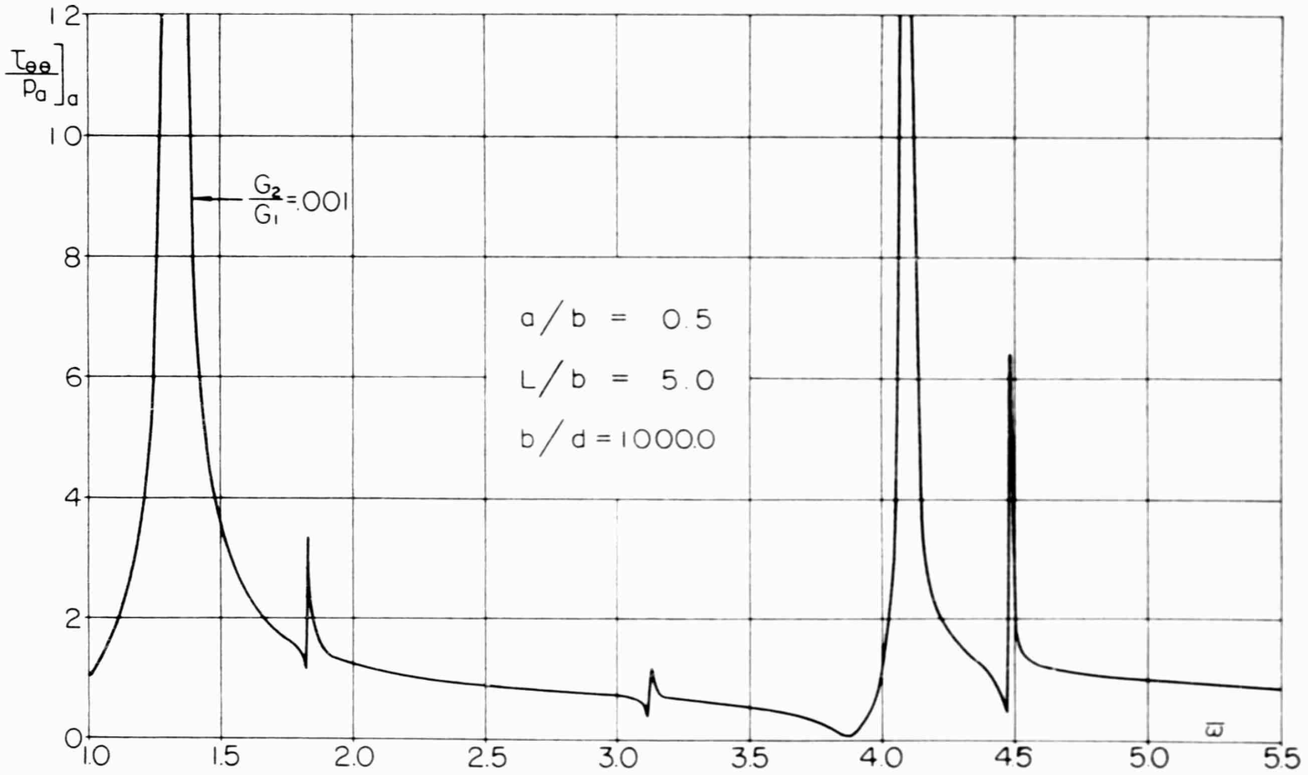

Figure 3b Absolute Value of Circumferential Stress at the Bore for Small Damping (a/b = .5 , b/d = 1000)

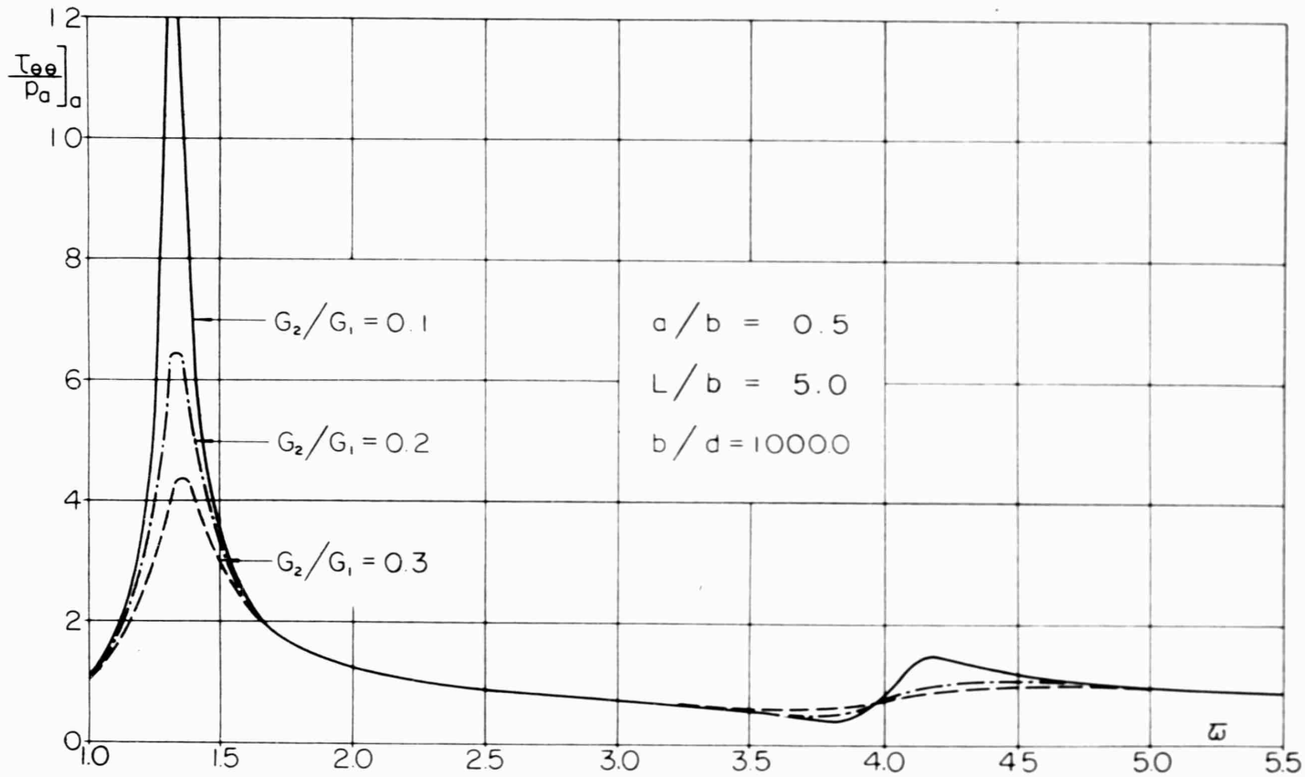

Figure 3c Absolute Value of Circumferential Stress at the Bore for Larger Damping (a/b = .5 , b/d = 1000)

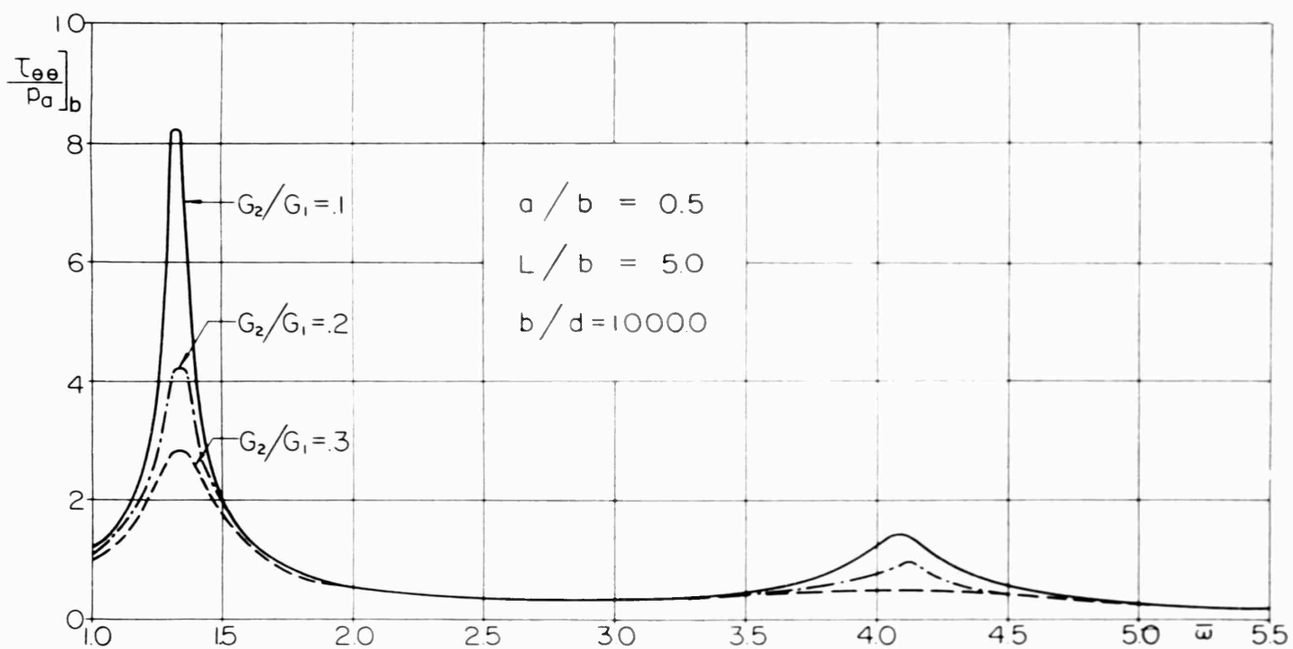

Figure 3d Absolute Value of Circumferential Stress at the Interface for Various Values of Damping (a/b = .5 , b/d = 1000)

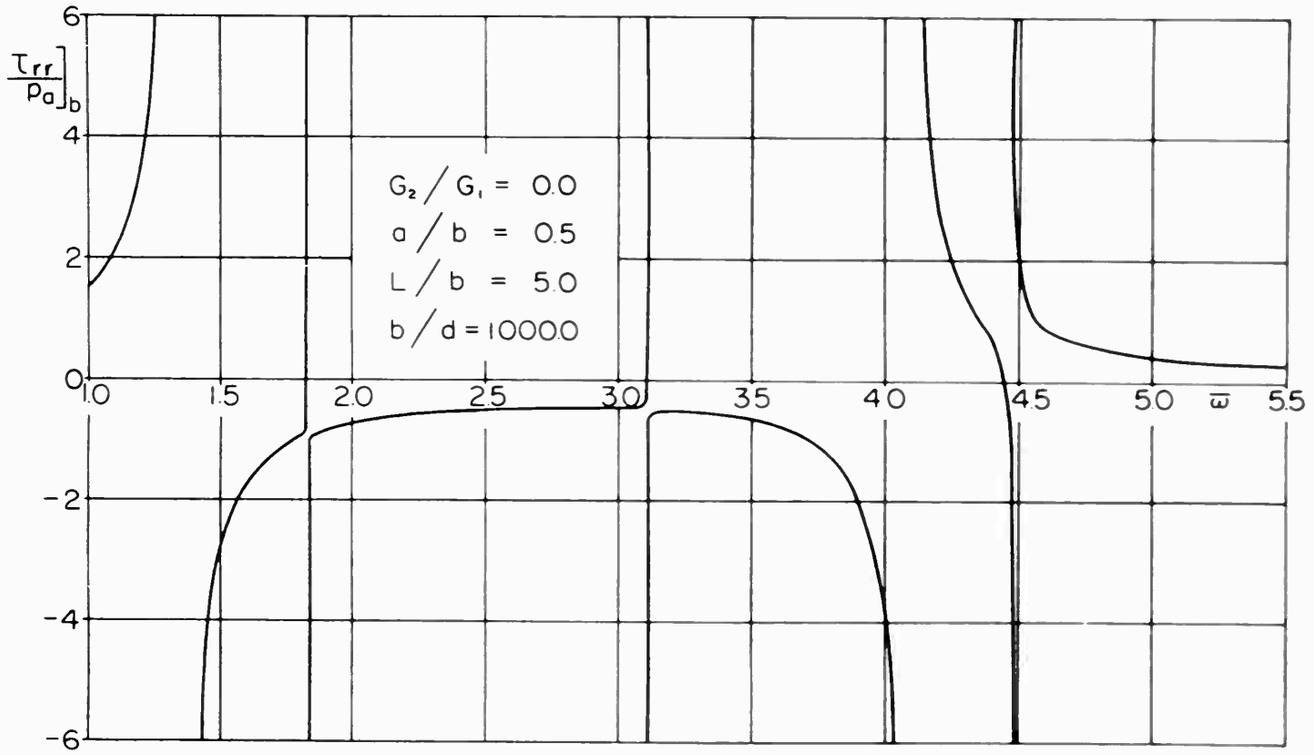

Figure 4a Radial Stress at the Interface for Elastic Cylinder and Shell ($a/b = .5$, $b/d = 1000$)

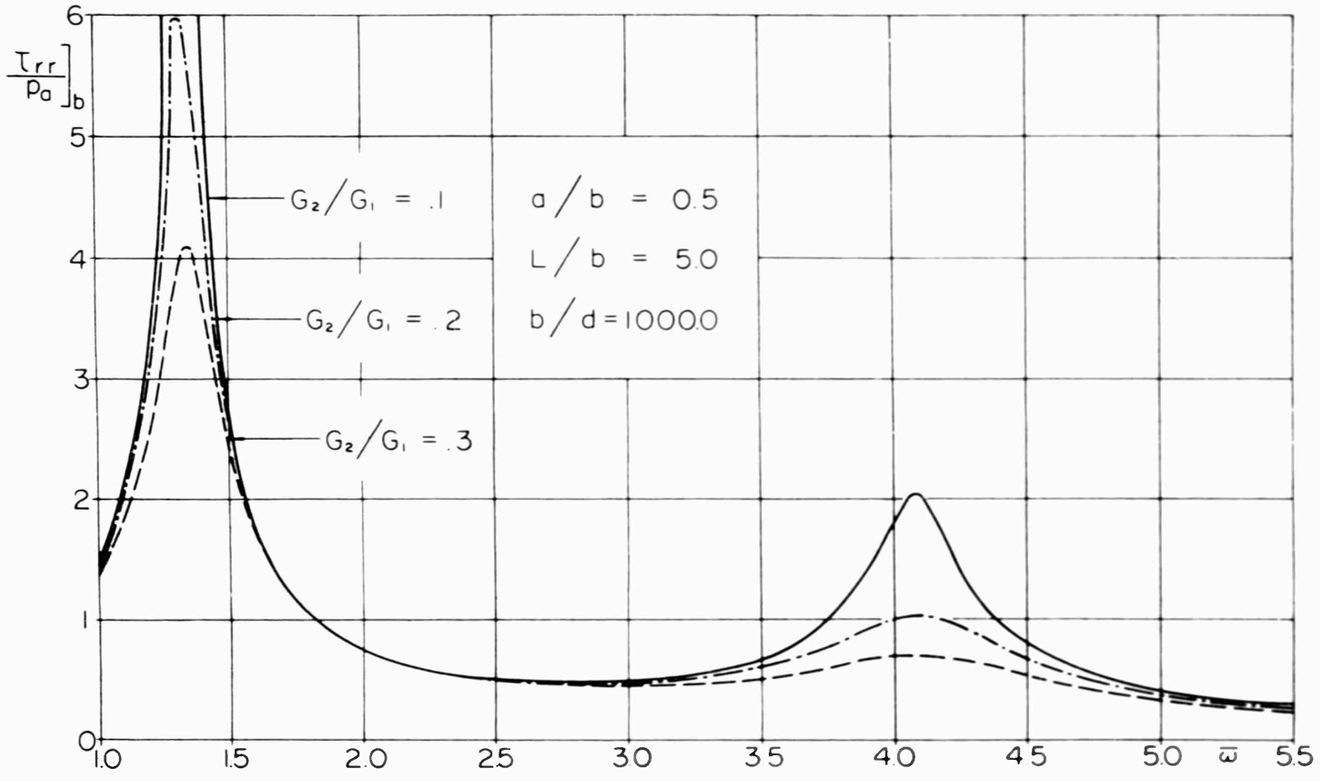

Figure 4b Absolute Value of Radial Stress at the Interface for Various Values of Damping (a/b = .5 , b/d = 1000)

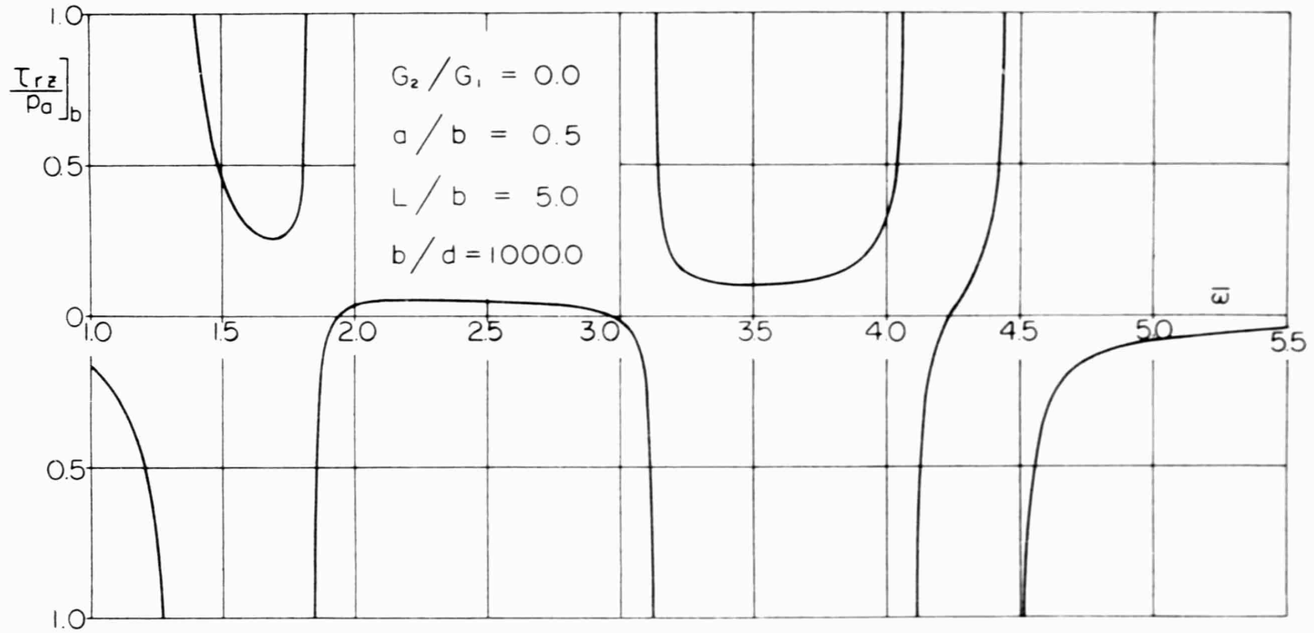

Figure 5a Shear Stress at the Interface for the Elastic Cylinder and Shell (a/b = .5 , b/d = 1000)

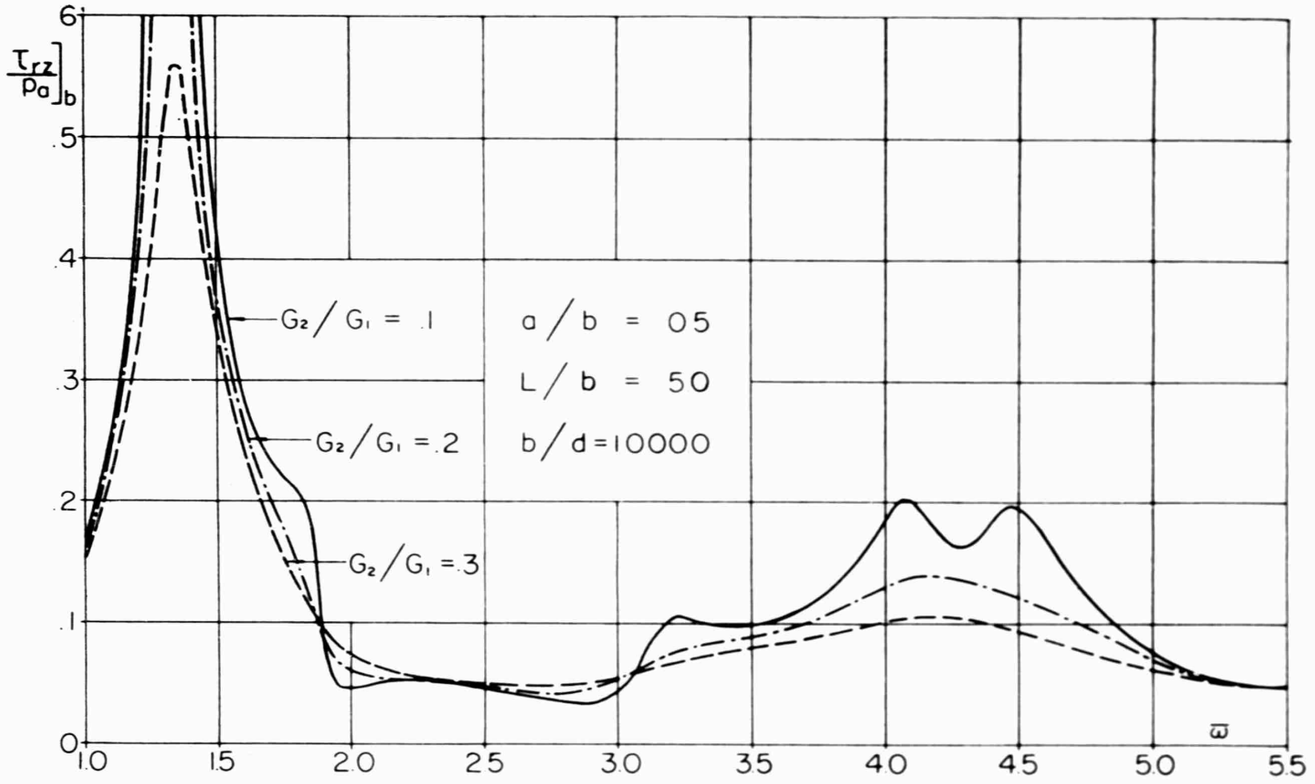

Figure 5b Absolute Value of Shear Stress at the Interface for Various Values of Damping (a/b = .5 , b/d = 1000)

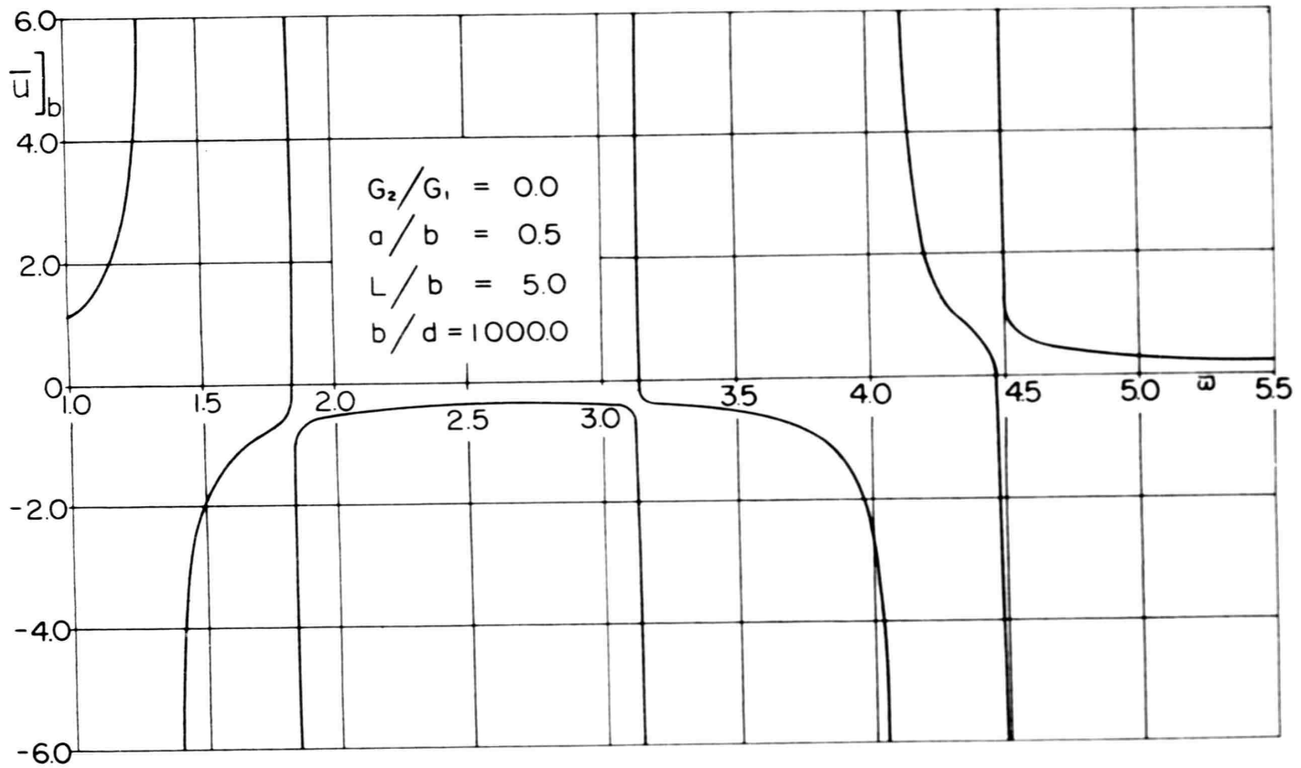

Figure 6a Radial Displacement $\bar{u}_r = 2Gu_r/dP_a$ at the Interface for the Elastic Cylinder and Shell ($a/b = .5$, $b/d = 1000$)

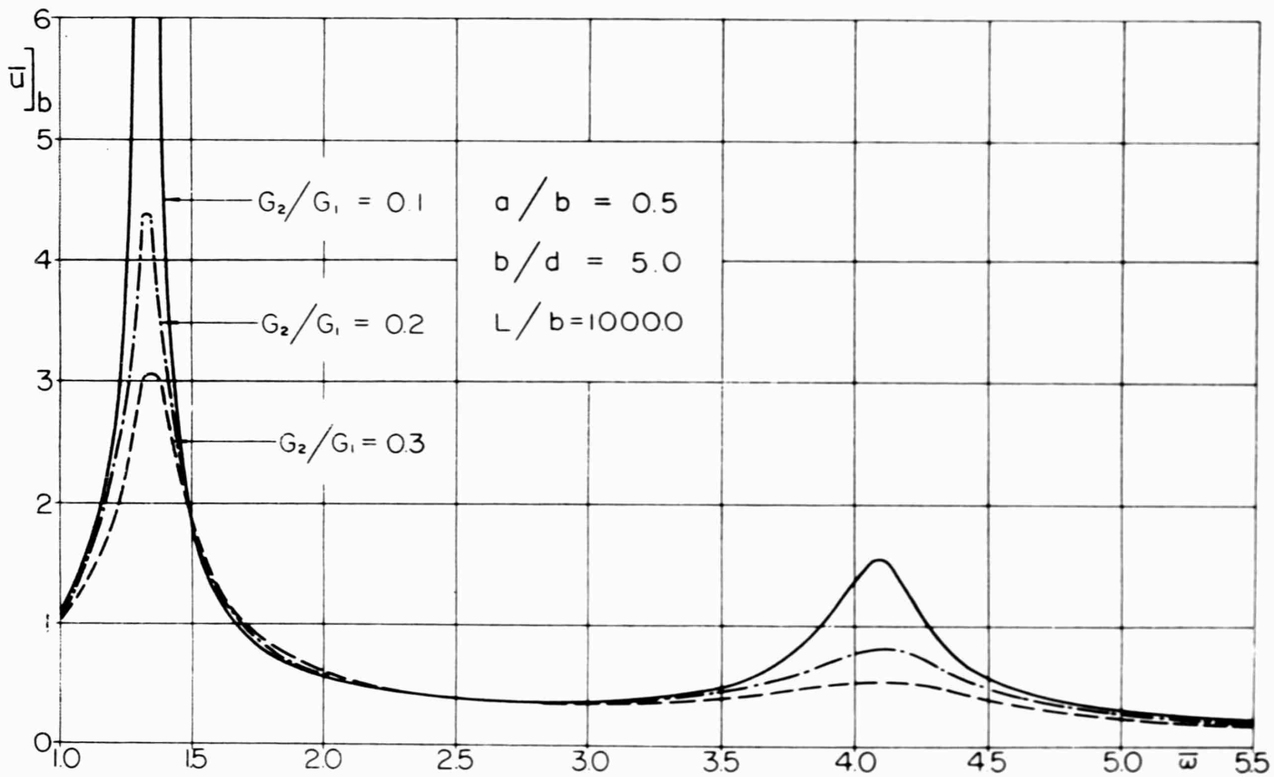

Figure 6b **Absolute Value of Radial Displacement at the Interface for Various Values of Damping** (a/b = .5 , b/d = 1000)

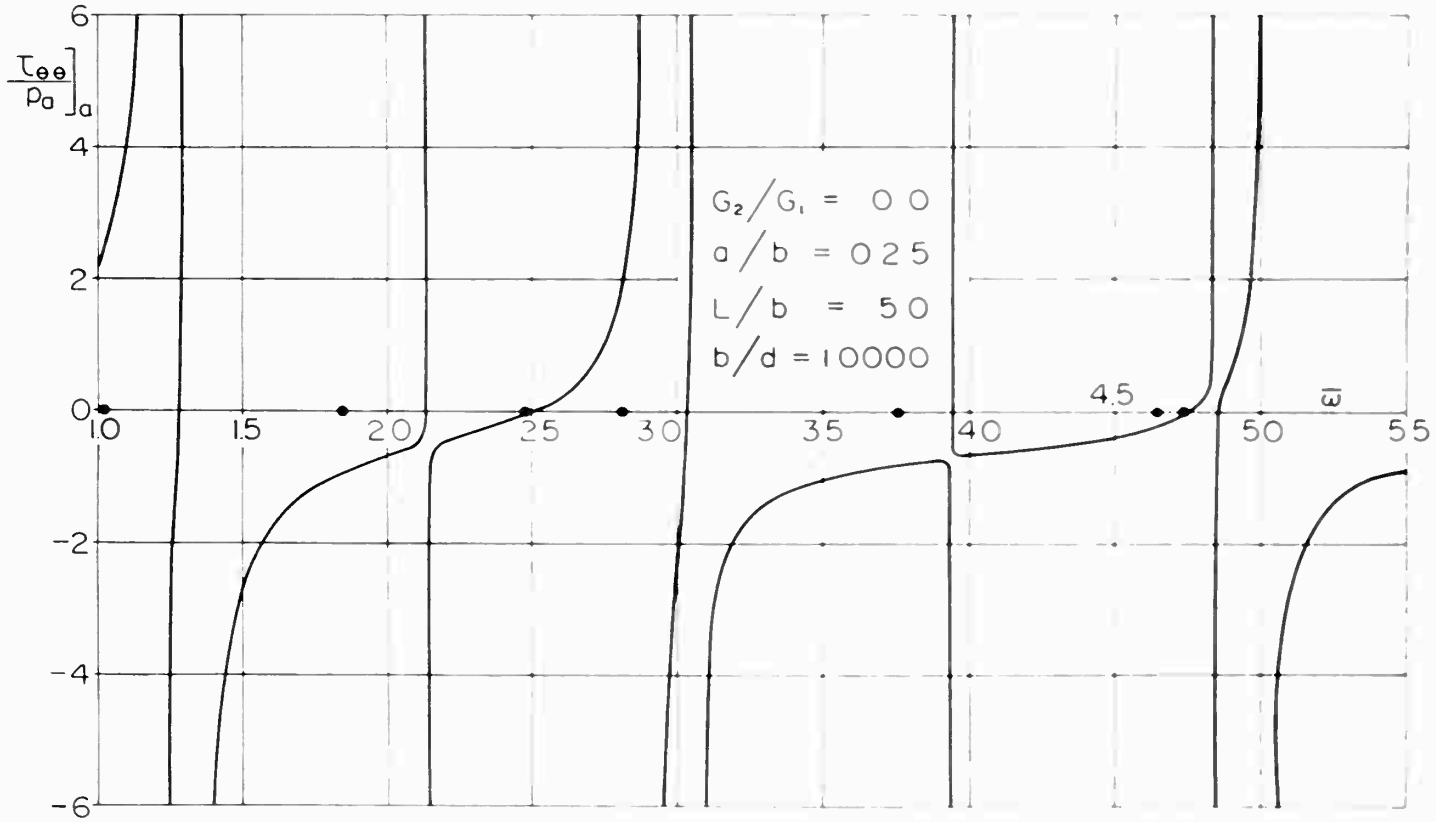

Figure 7a Circumferential Stress at the Bore for the Elastic Cylinder and Shell and also Showing Roots of the Frequency Equation for the Cylinder Alone

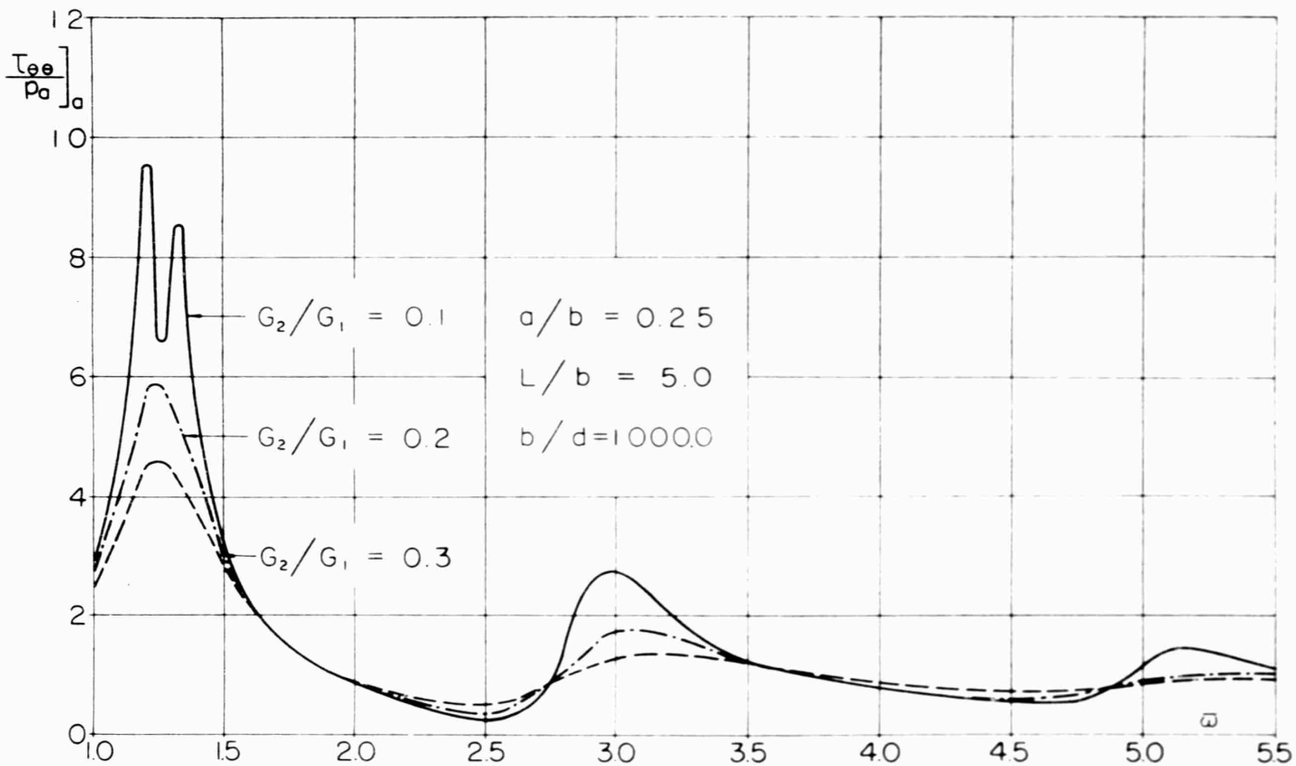

Figure 7b Absolute Value of Circumferential Stress at the Bore for Various Values of Damping and Indicated Values of Parameters

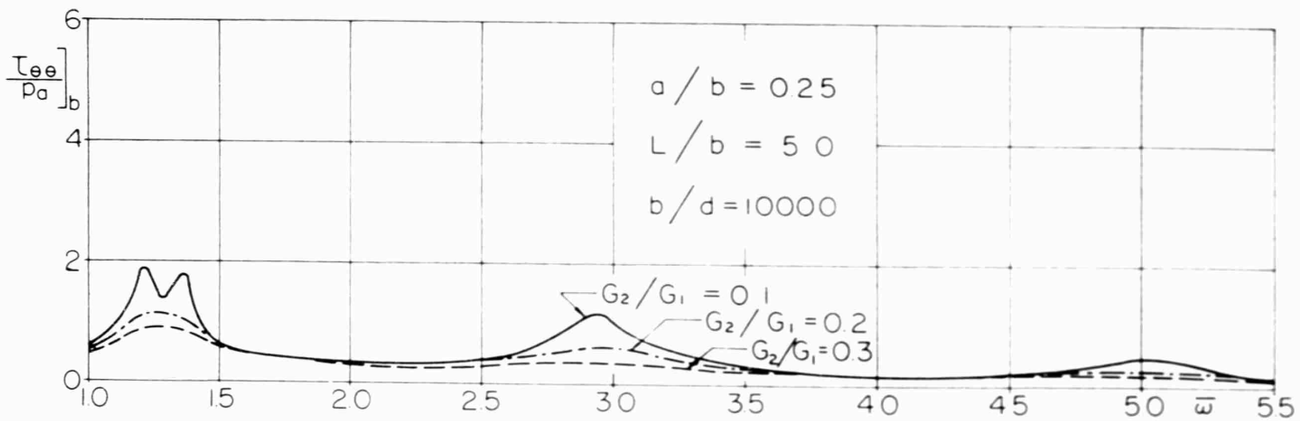

Figure 7c Absolute Value of Circumferential Stress at the Interface for Various Values of Damping and Indicated Values of Parameters.

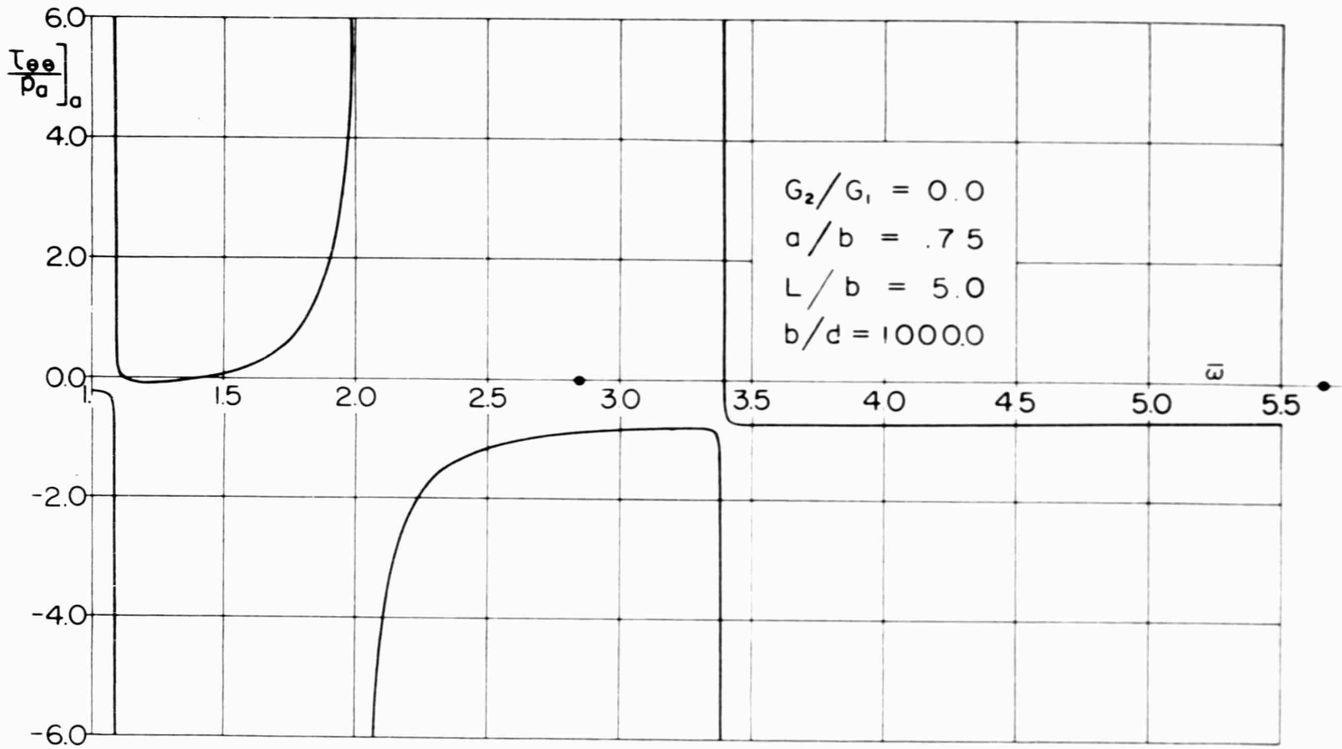

Figure 8a Circumferential Stress at the Bore for the Elastic Cylinder and Shell and also Showing Roots of the Frequency Equation for the Cylinder Alone

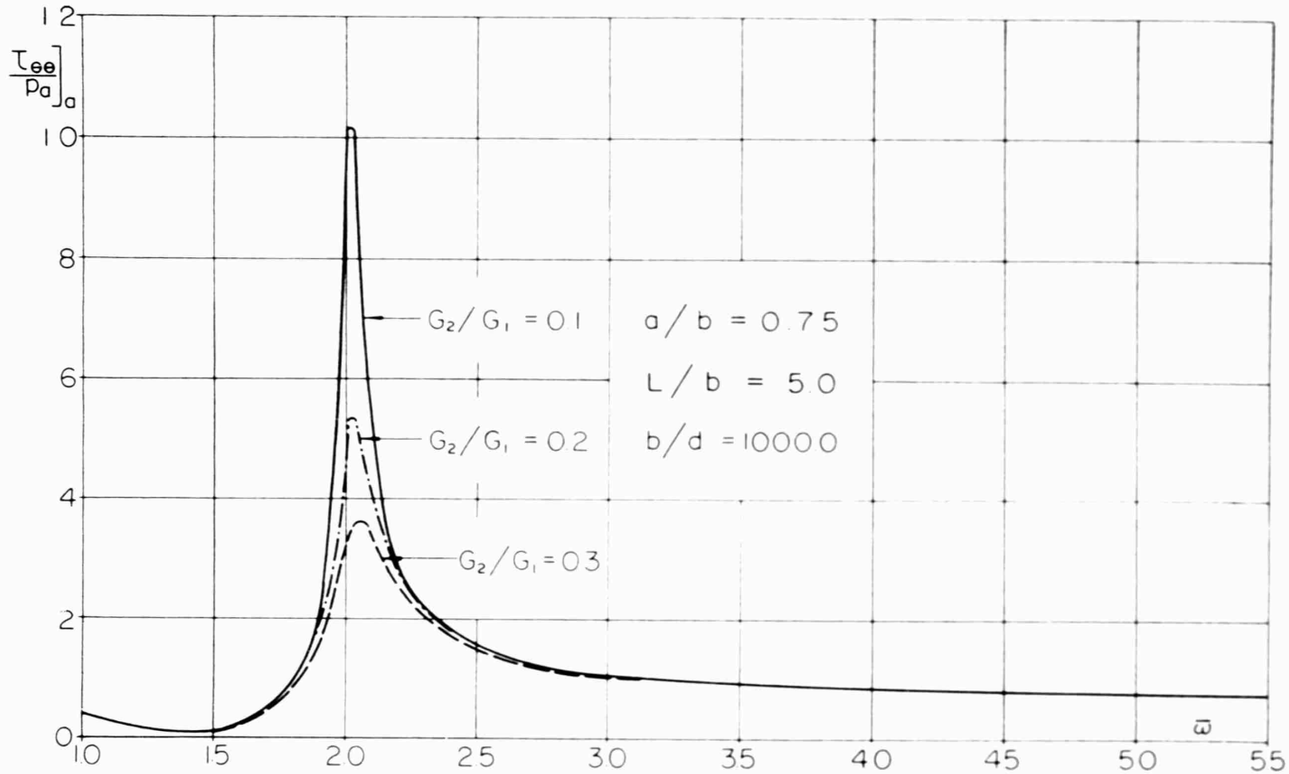

Figure 8b Absolute Value of Circumferential Stress at the Bore for Various Values of Damping and Indicated Values of Parameters

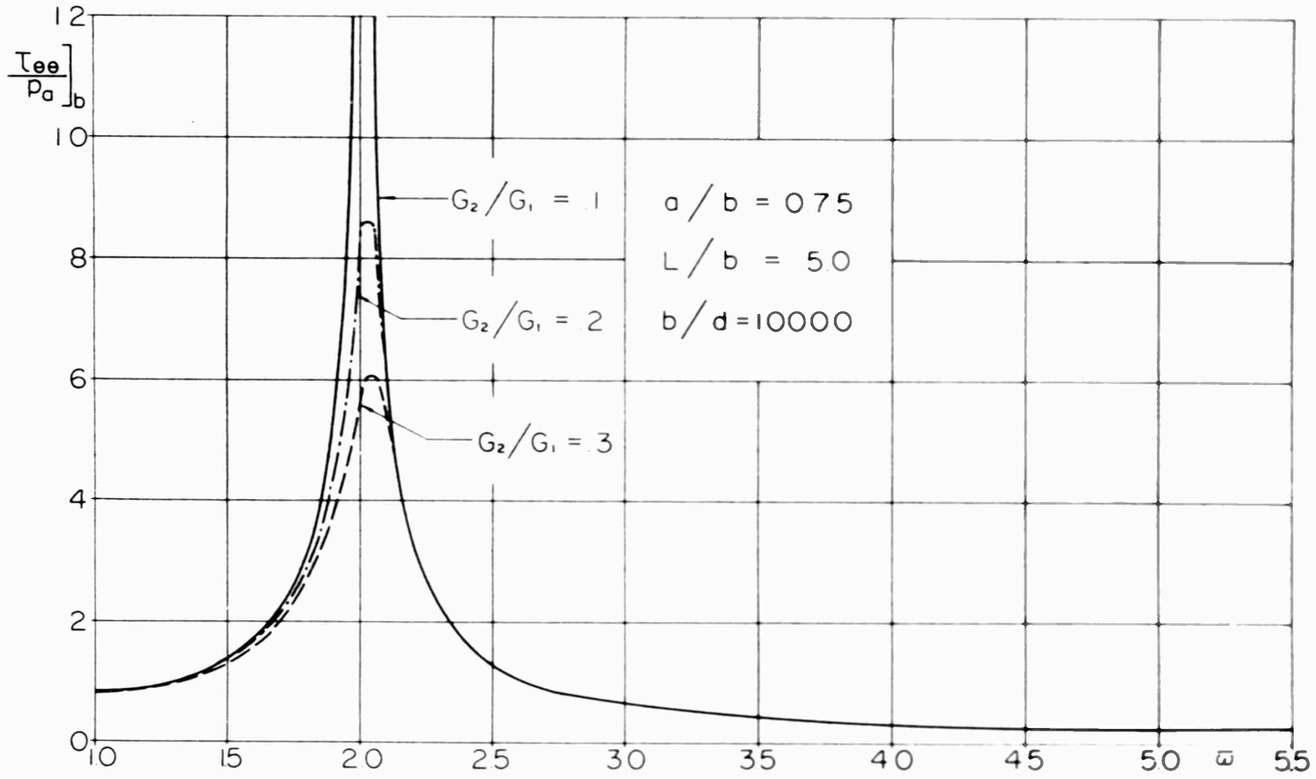

Figure 8c Absolute Value of Circumferential Stress at the Interface for Various Values of Damping and Indicated Values of Parameters

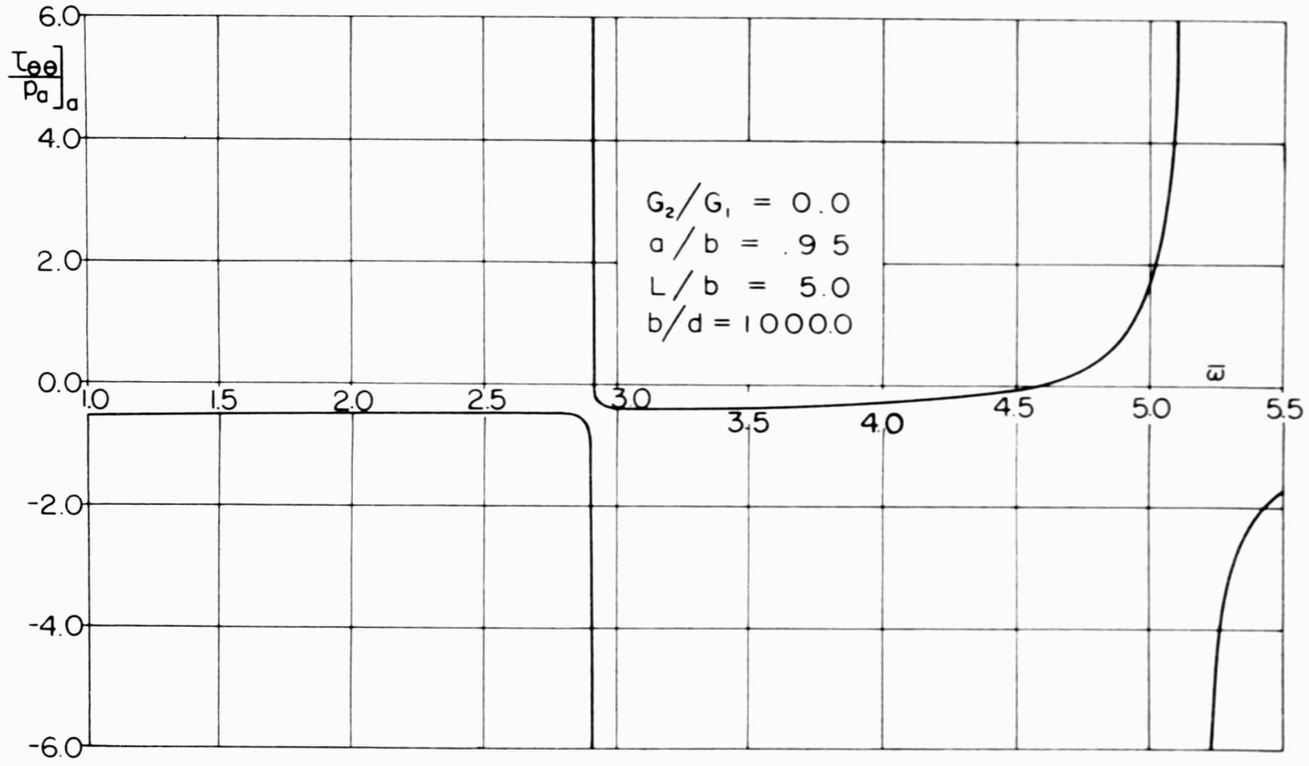

Figure 9a A Circumferential Stress at the Bore for the Elastic Cylinder and Shell and Parameters as Indicated

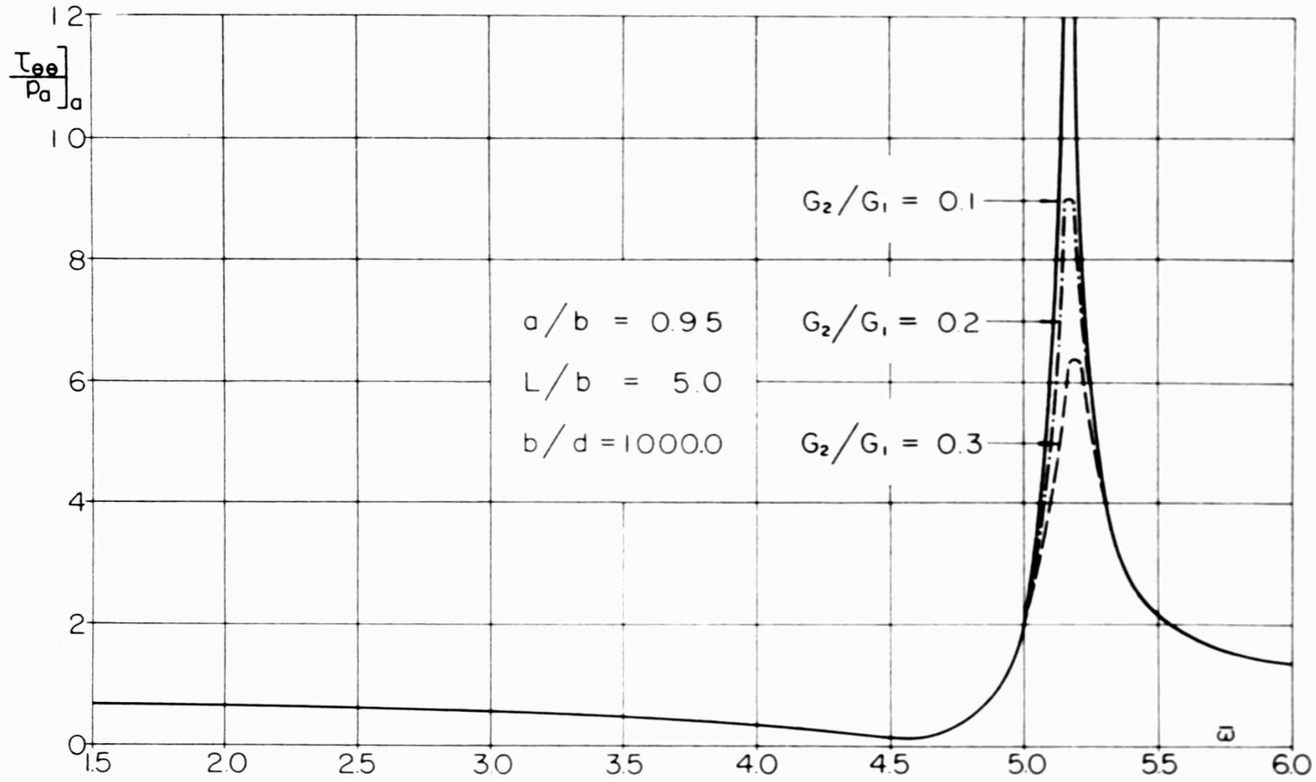

Figure 9b Absolute Value of Circumferential Stress at the Bore for Various Values of Damping and Parameters as Indicated

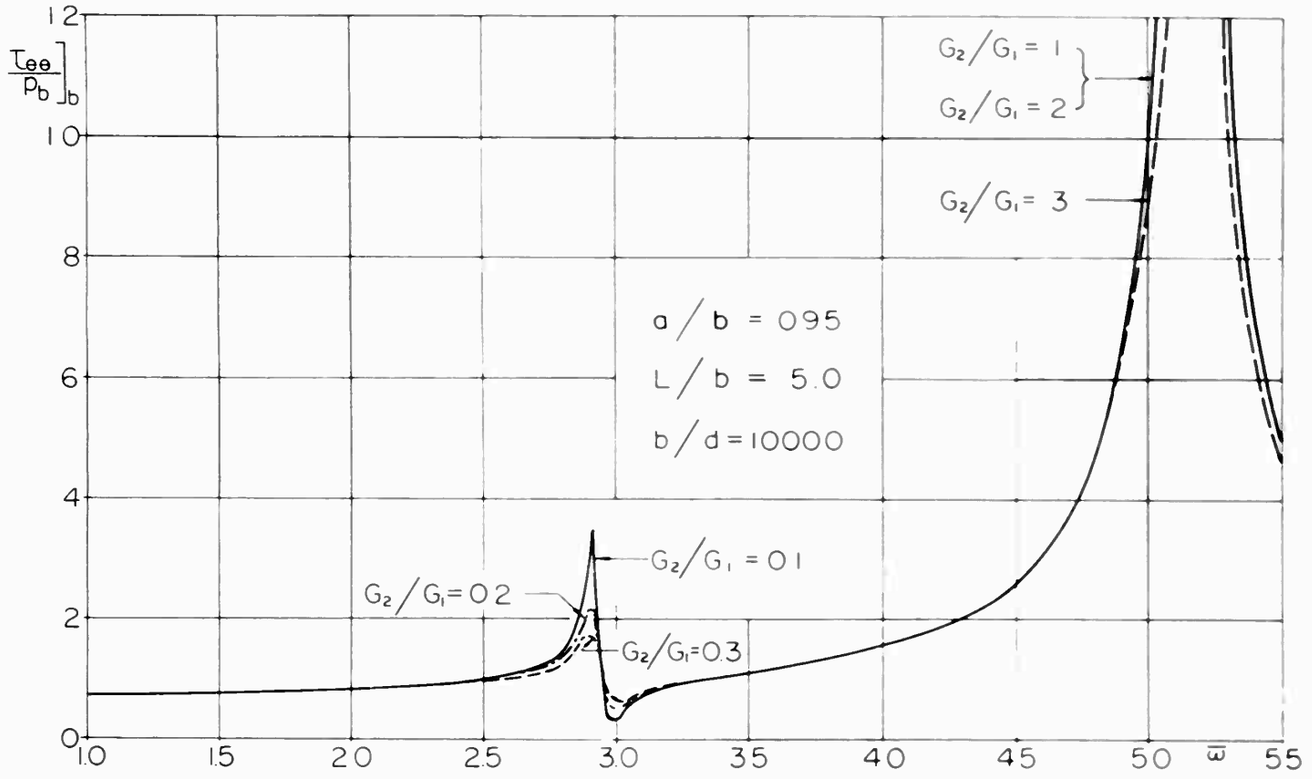

Figure 3c Absolute Value of Circumferential Stress at the Interface for Various Values of Damping and Parameters as Indicated.

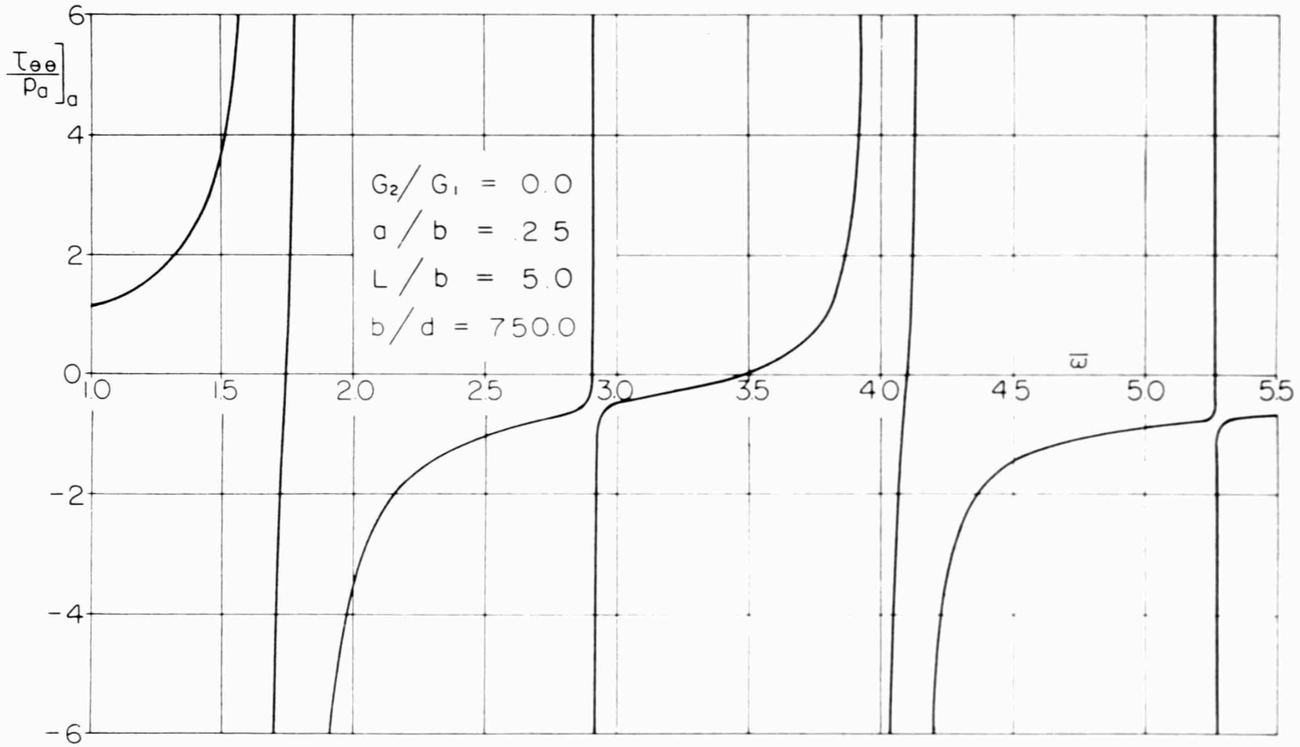

Figure 10a A Circumferential Stress at the Bore for the Elastic Cylinder and Shell and Parameters as Indicated

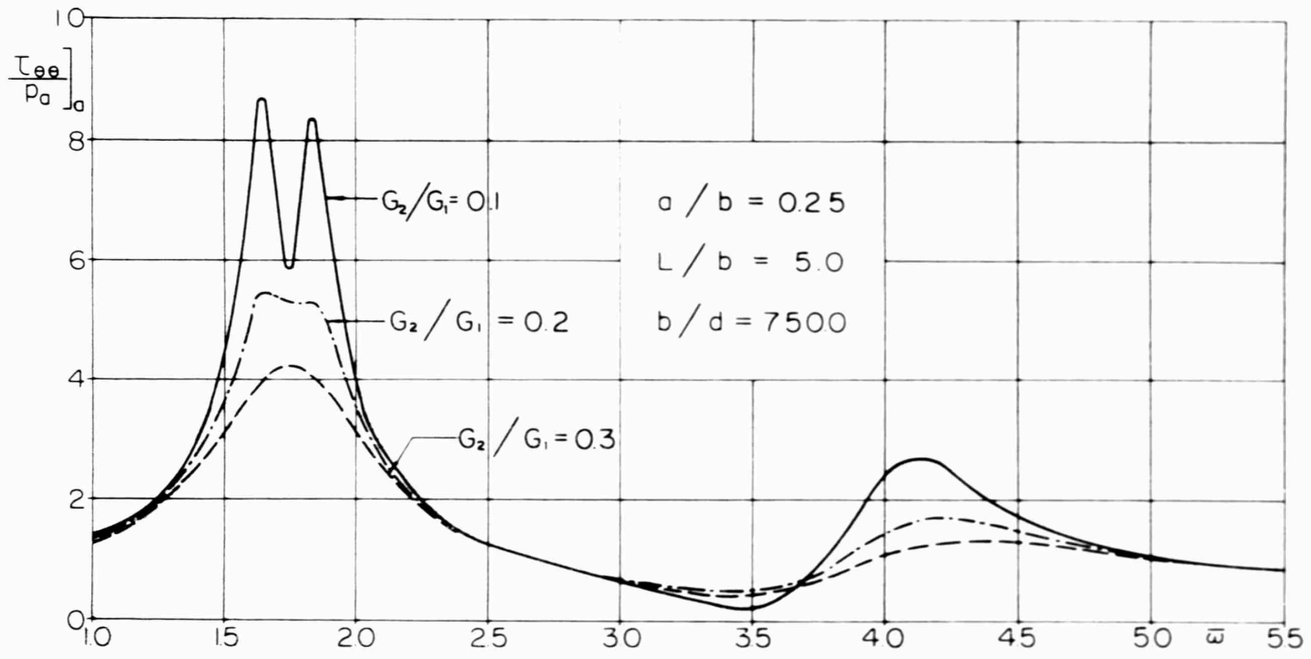

Figure 10b Absolute Value of Circumferential Stress at the Bore for Various Values of Damping and Parameters as Indicated

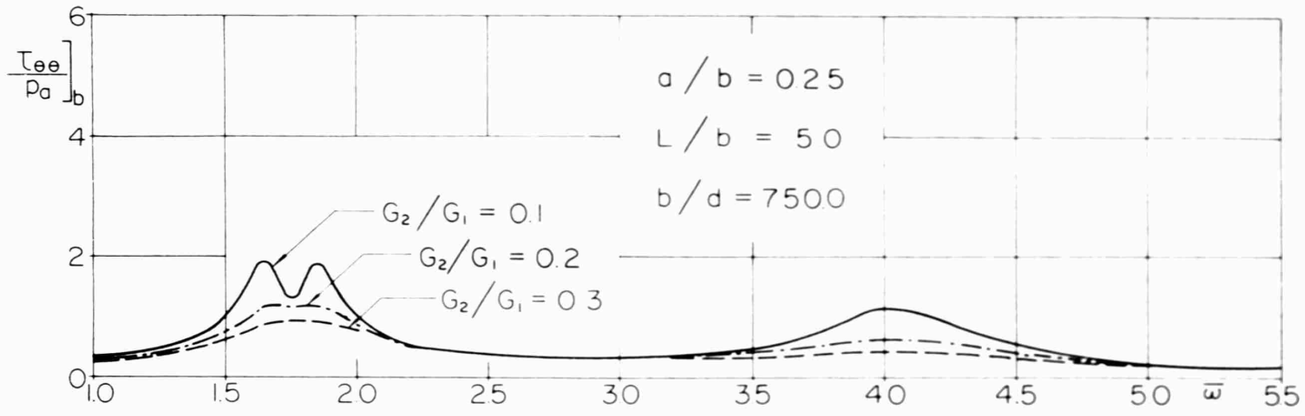

Figure 10c Absolute Value of Circumferential Stress at the Interface for Various Values of Damping and Parameters as Indicated

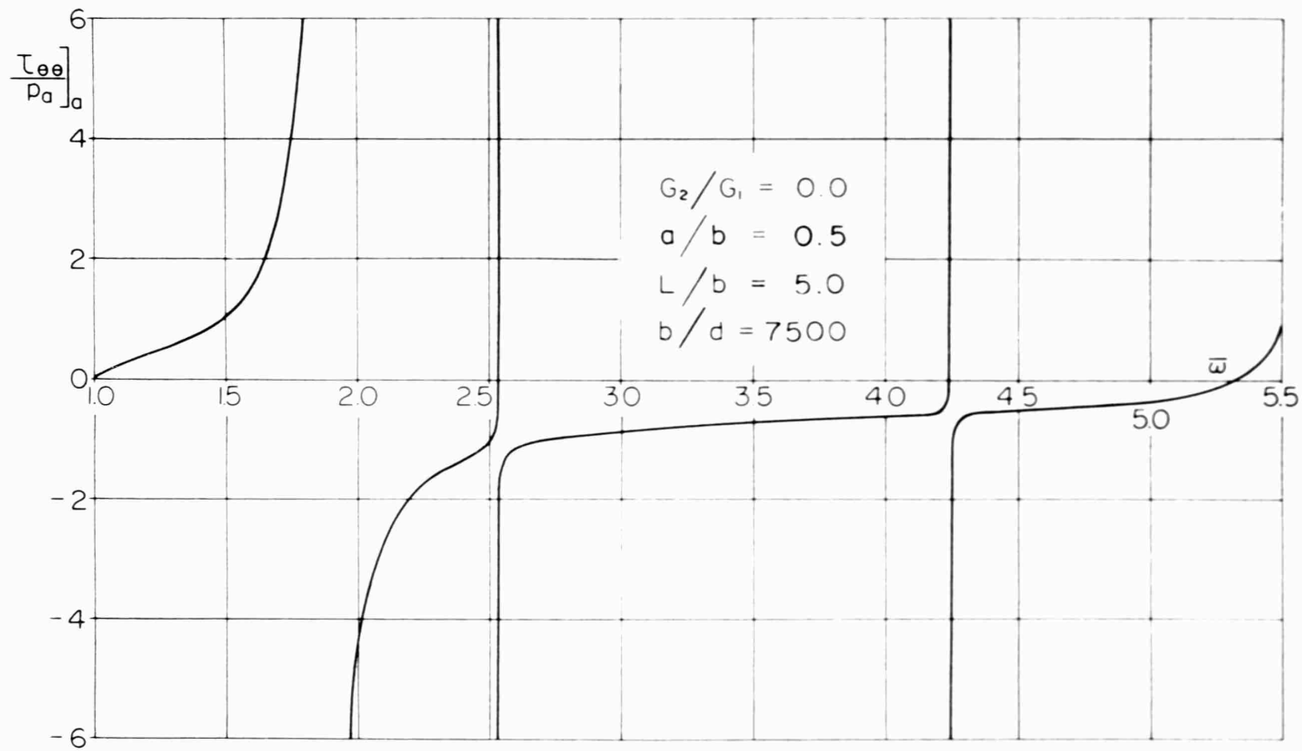

Figure 11a Circumferential Stress at the Bore for the Elastic Cylinder and Shell and Parameters as Indicated

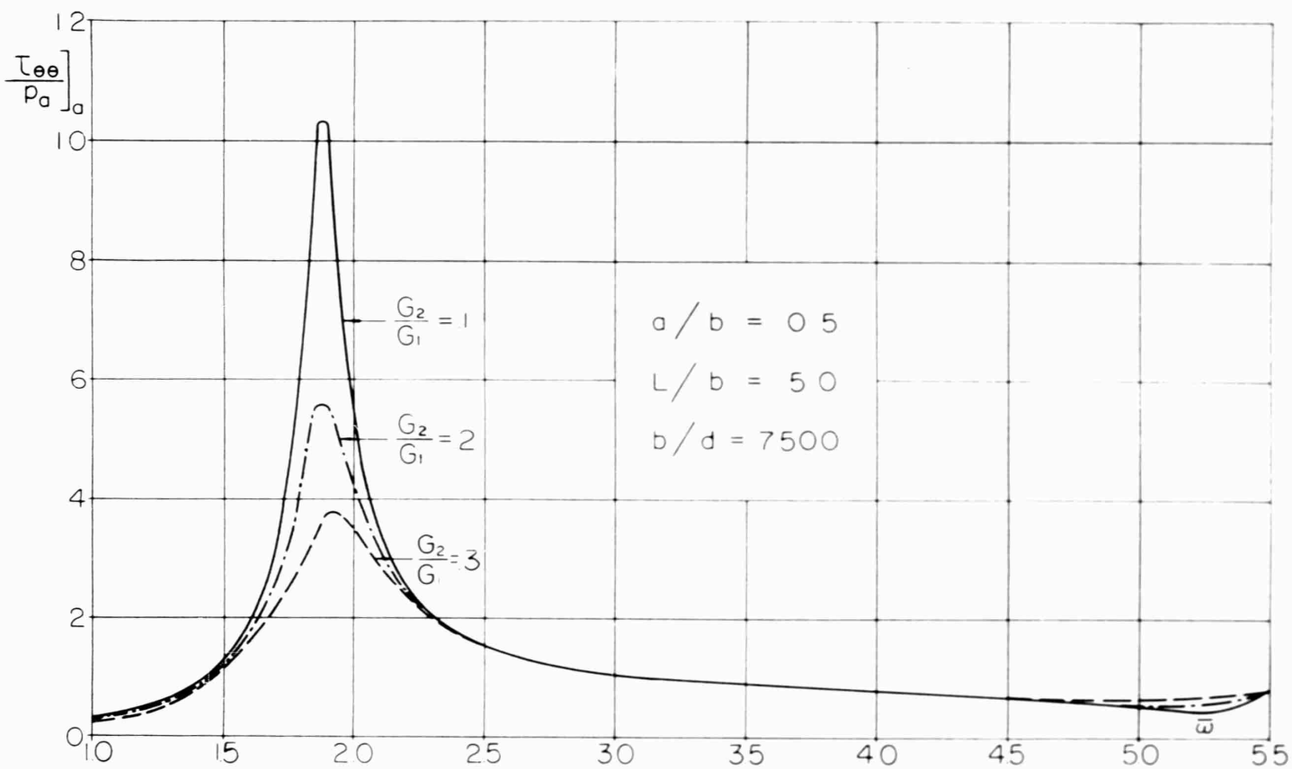

Figure 11b Absolute Value of Circumferential Stress at the Bore for Various Values of Damping and Parameters as Indicated

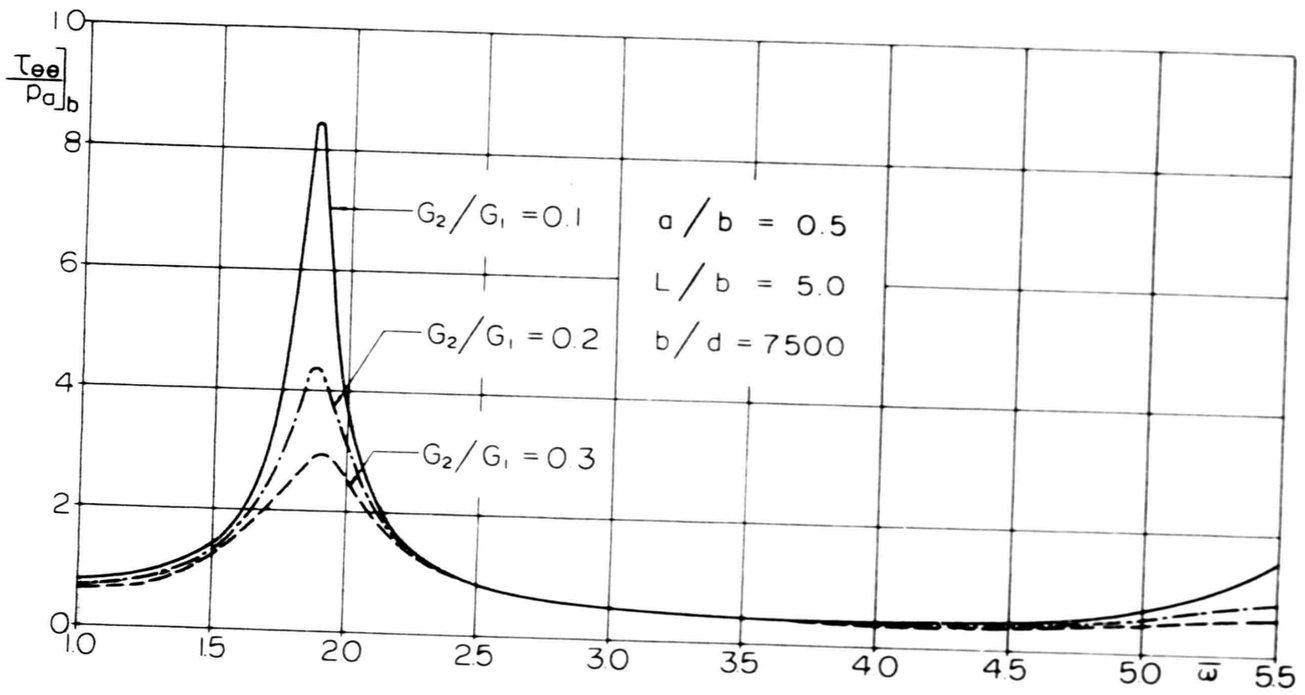

Figure 11c Absolute Value of Circumferential Stress at the Interface for Various Values of Damping and Parameters as Indicated

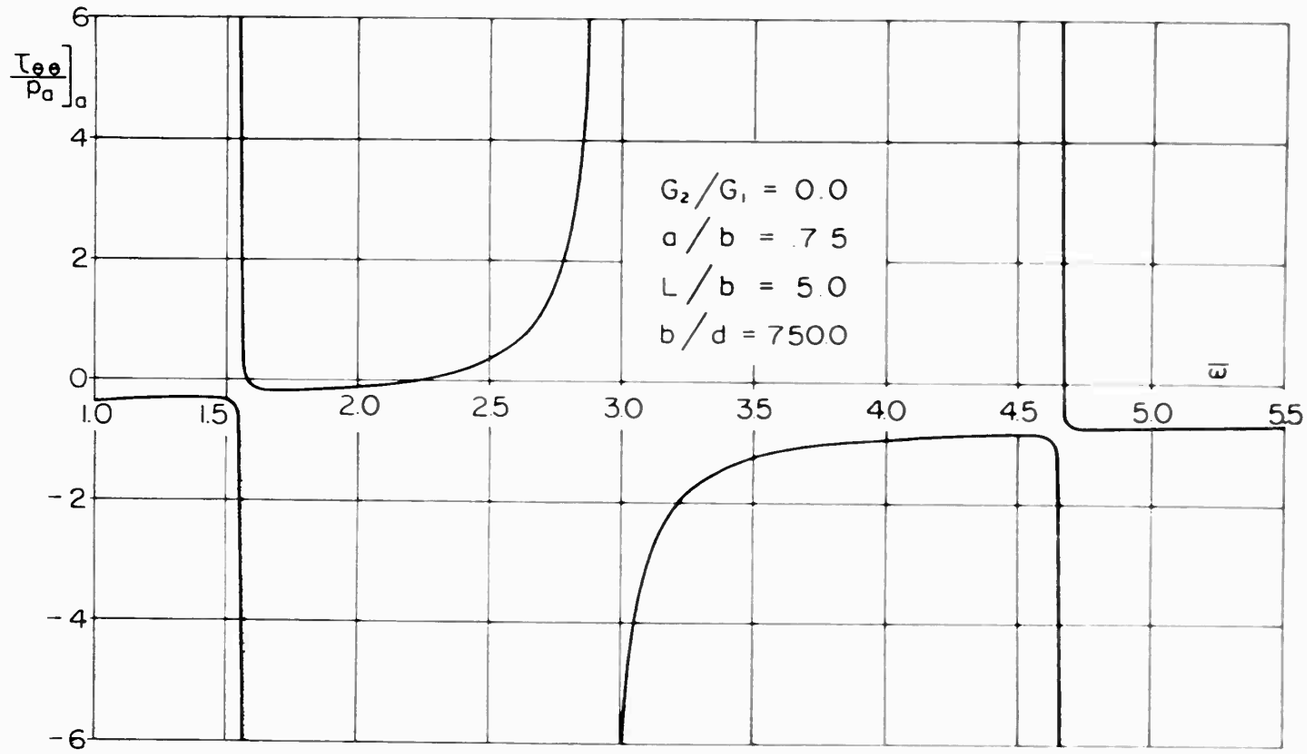

Figure 12a Circumferential Stress at the Bore for the Elastic Cylinder and Shell and Parameters as Indicated

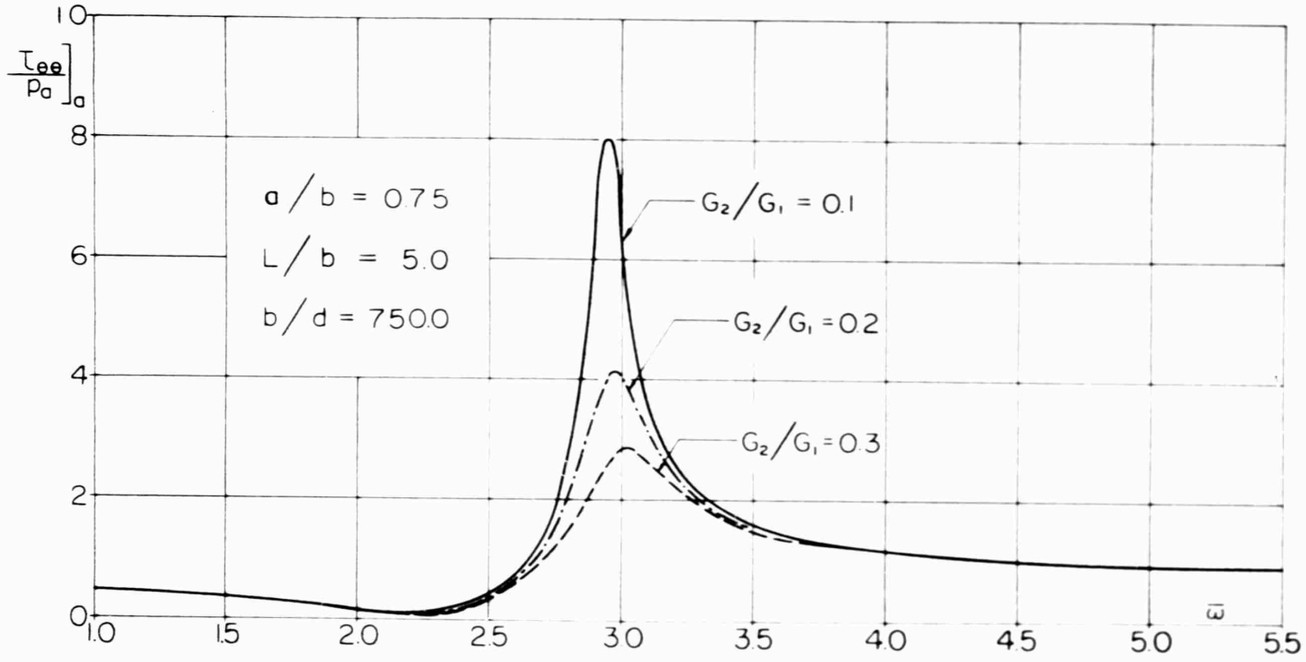

Figure 12b Absolute Value of Circumferential Stress at the Bore for Various Values of Damping and Parameters as Indicated

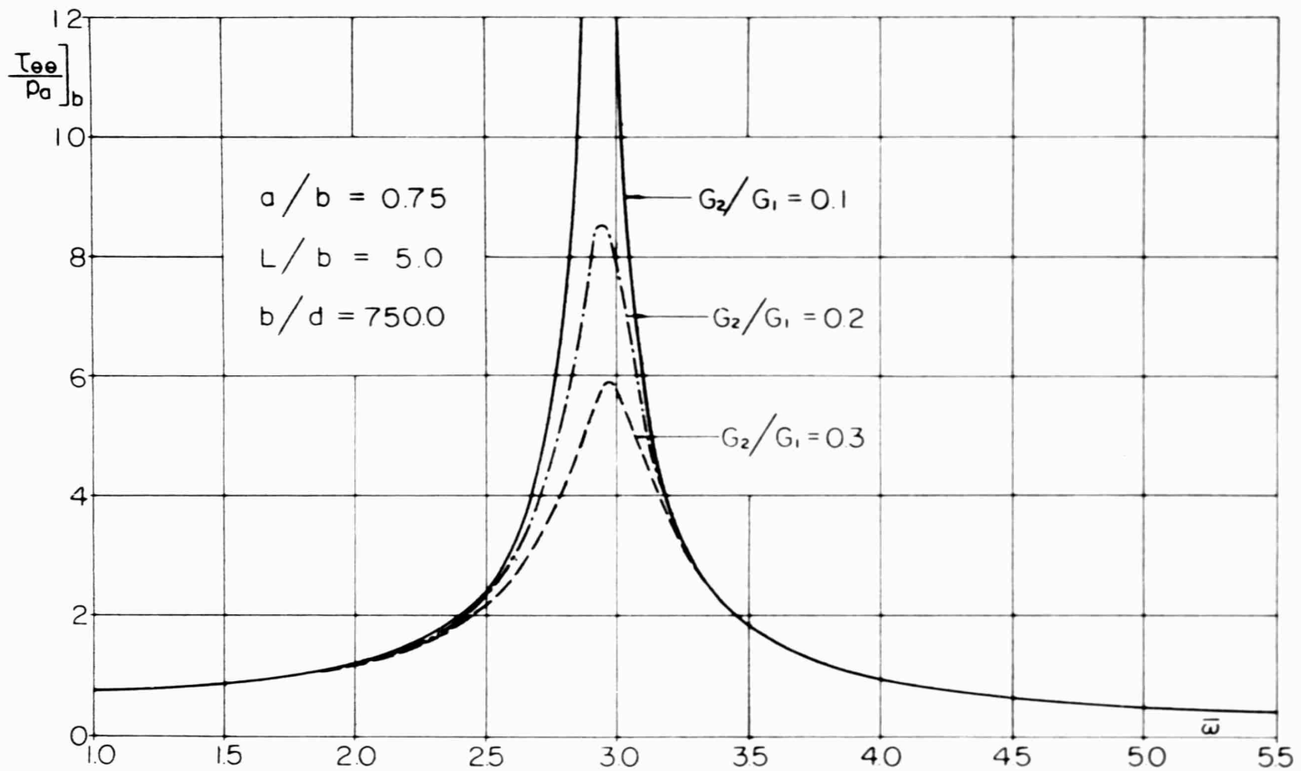

Figure 12c Absolute Value of Circumferential Stress at the Interface for Various Values of Damping and Parameters as Indicated

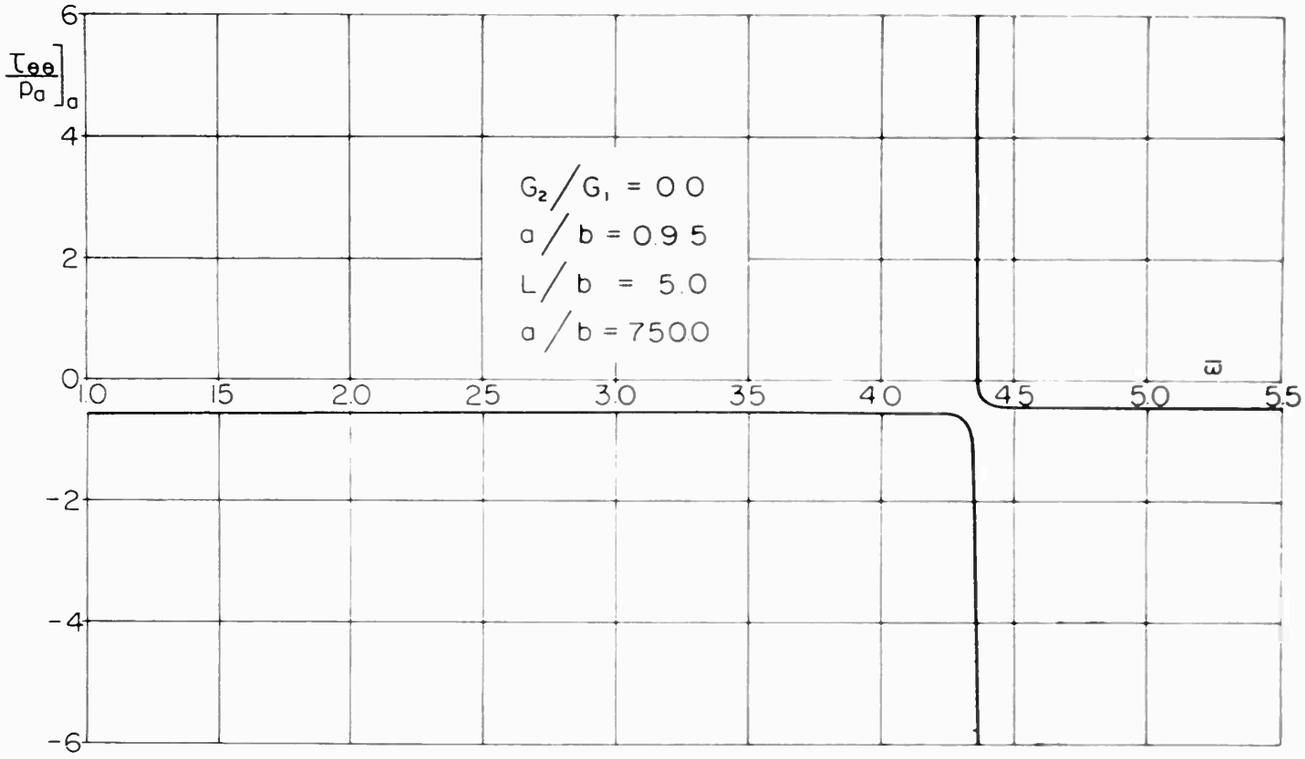

Figure 13a Circumferential Stress at the Bore for the Elastic Cylinder and Shell and Parameters as Indicated

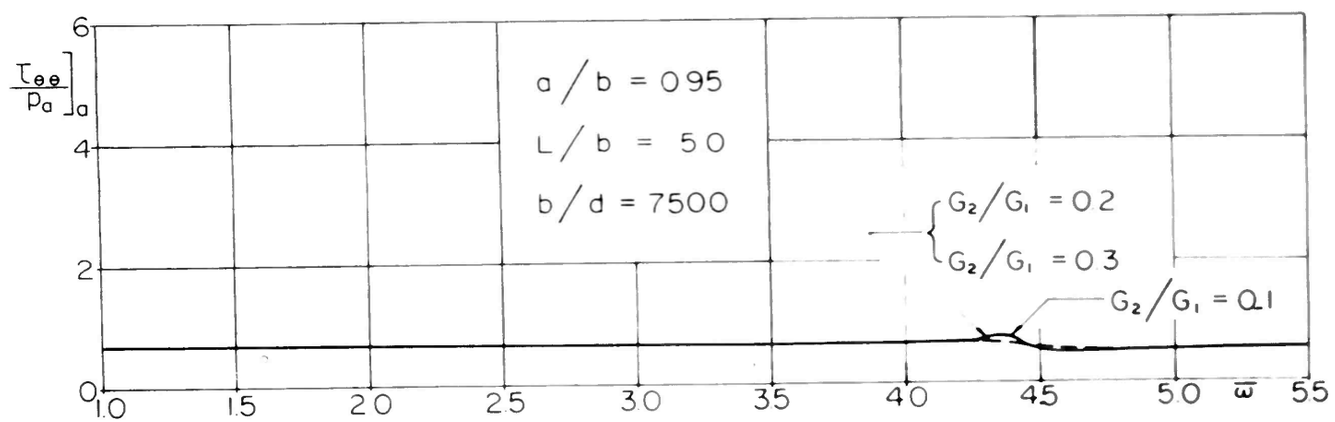

Figure 13b Absolute Value of Circumferential Stress at the Bore for Various Values of Damping and Parameters as Indicated

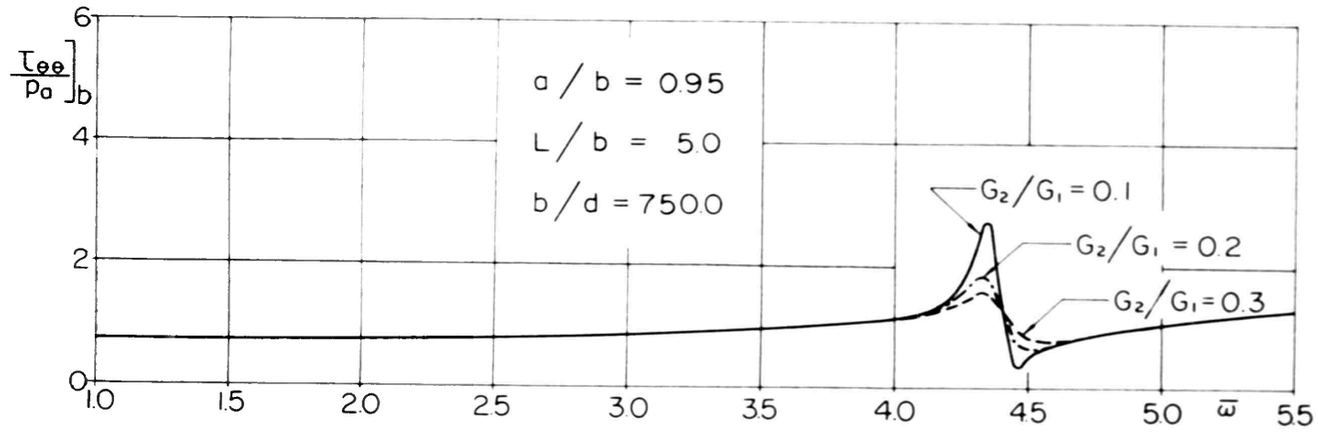

Figure 13c Absolute Value of Circumferential Stress at the Interface for Various Values of Damping and Parameters as Indicated

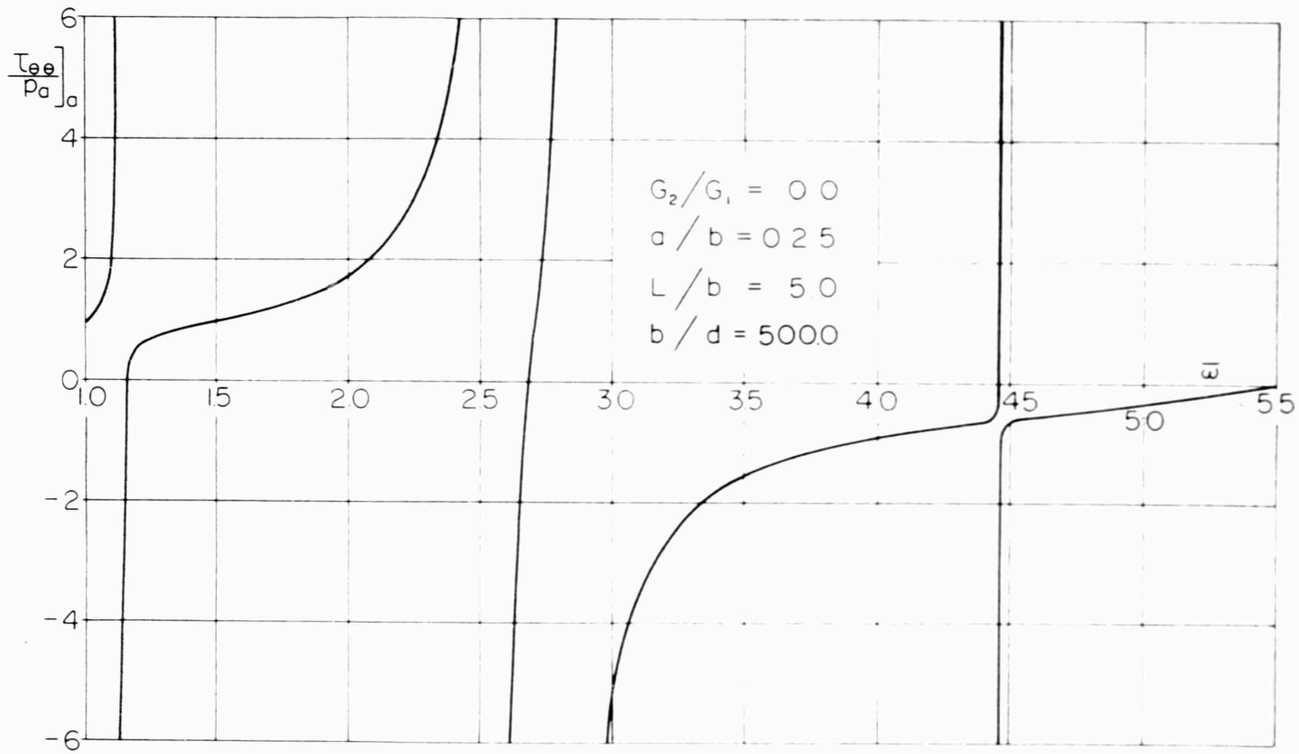

Figure 14a Circumferential Stress at the Bore for the Elastic Cylinder and Shell and Parameters as Indicated

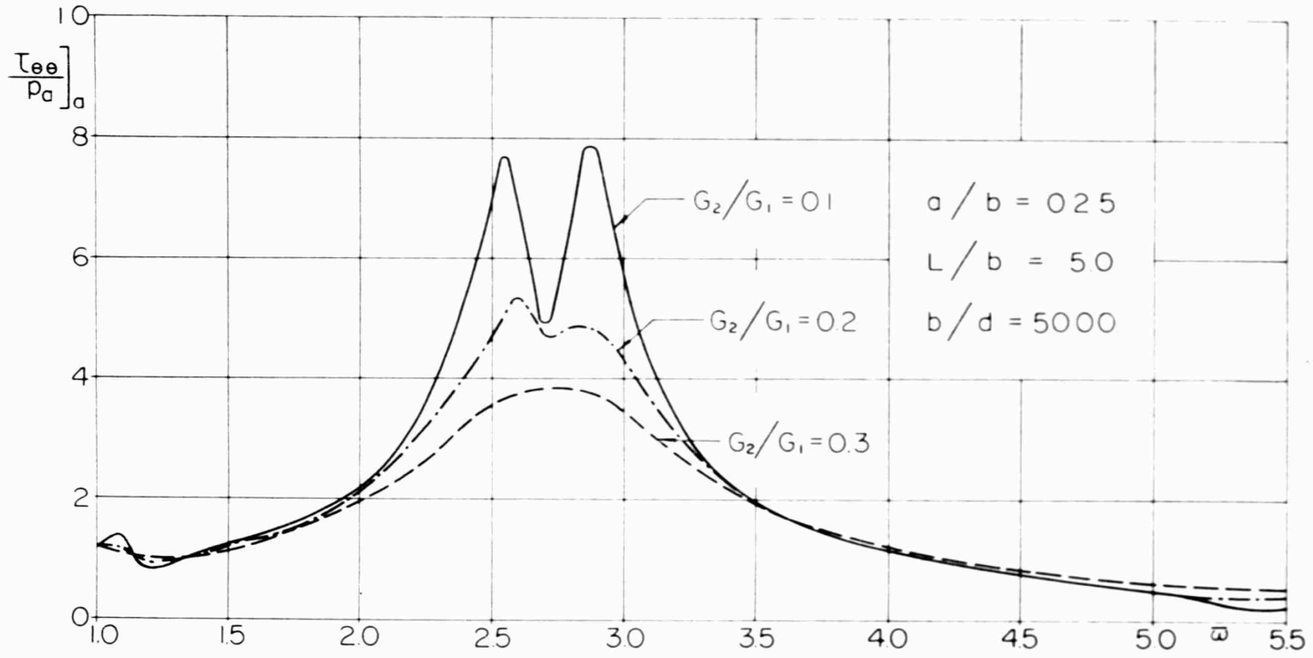

Figure 14b Absolute Value of Circumferential Stress at the Bore for Various Values of Damping and Parameters as Indicated

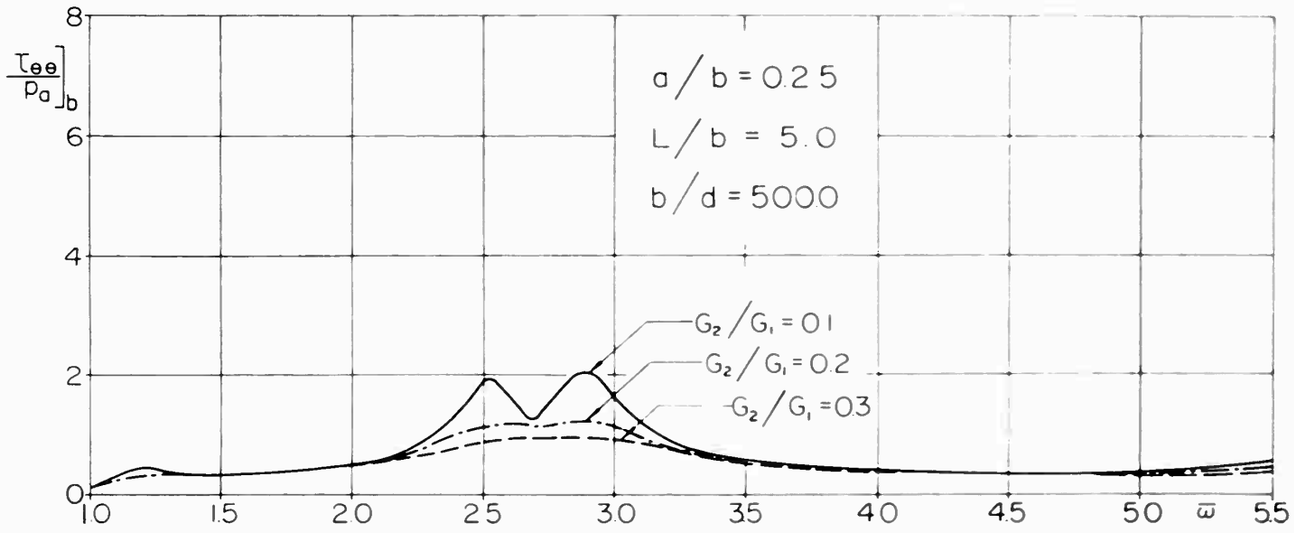

Figure 14c Absolute Value of Circumferential Stress at the Interface for Various Values of Damping and Parameters as Indicated

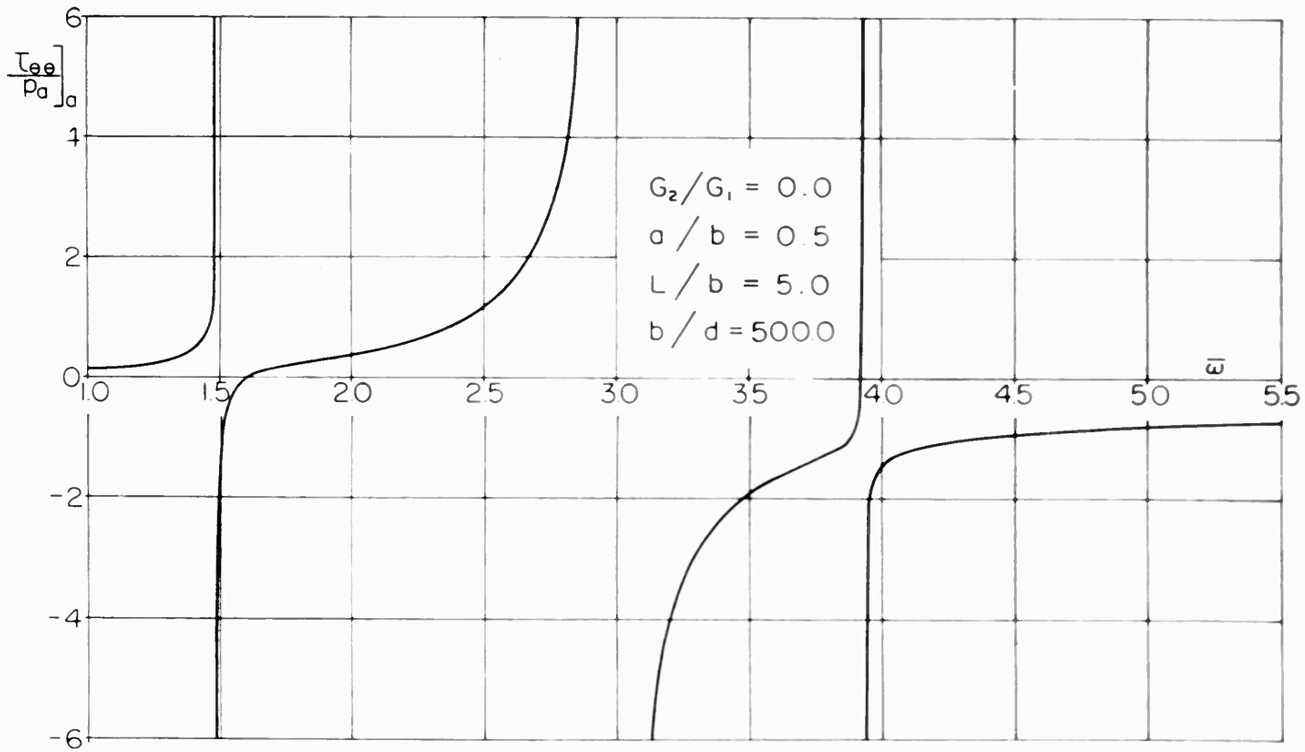

Figure 15a Circumferential Stress at the Bore for the Elastic Cylinder and Shell and Parameters as Indicated

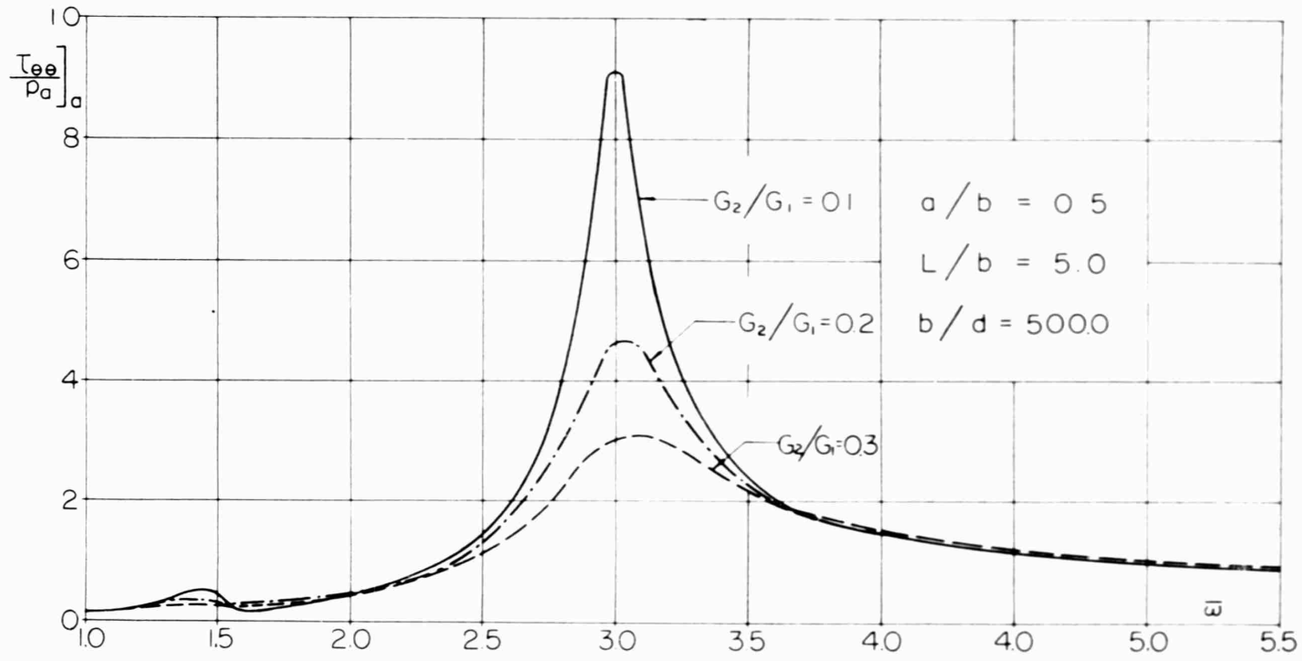

Figure 15b Absolute Value of Circumferential Stress at the Bore for Various Values of Damping and Parameters as Indicated

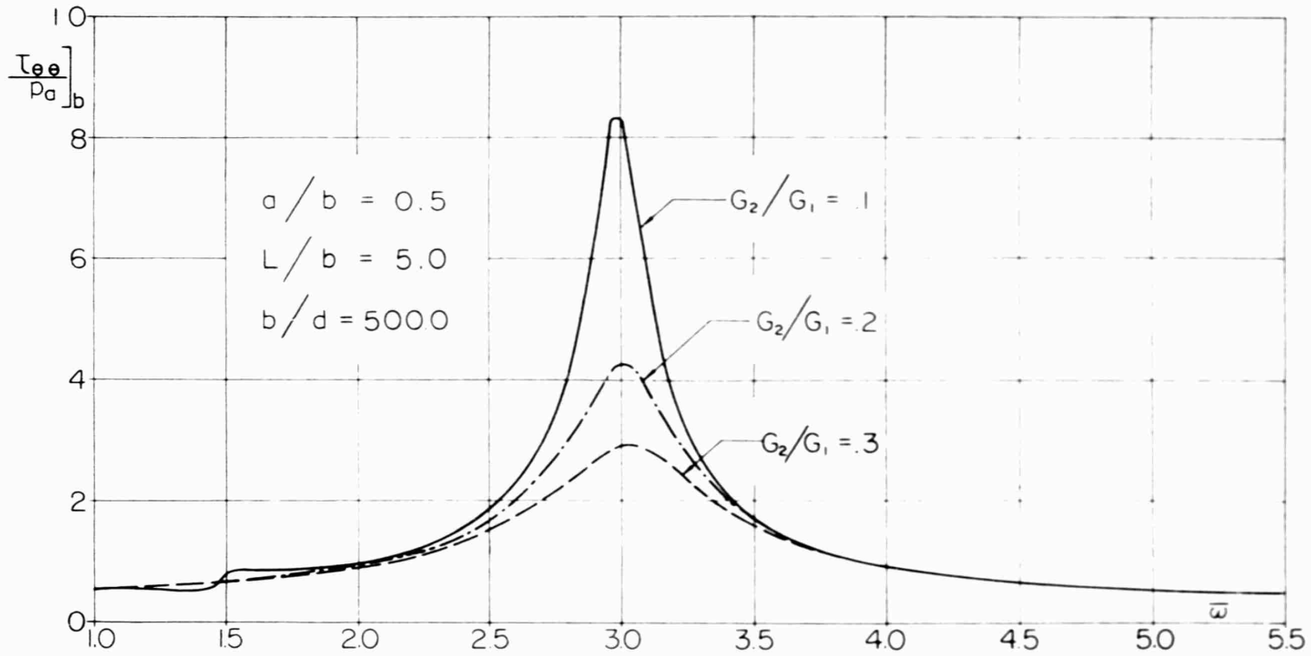

Figure 15c Absolute Value of Circumferential Stress at the Interface for Various Values of Damping and Parameters as Indicated

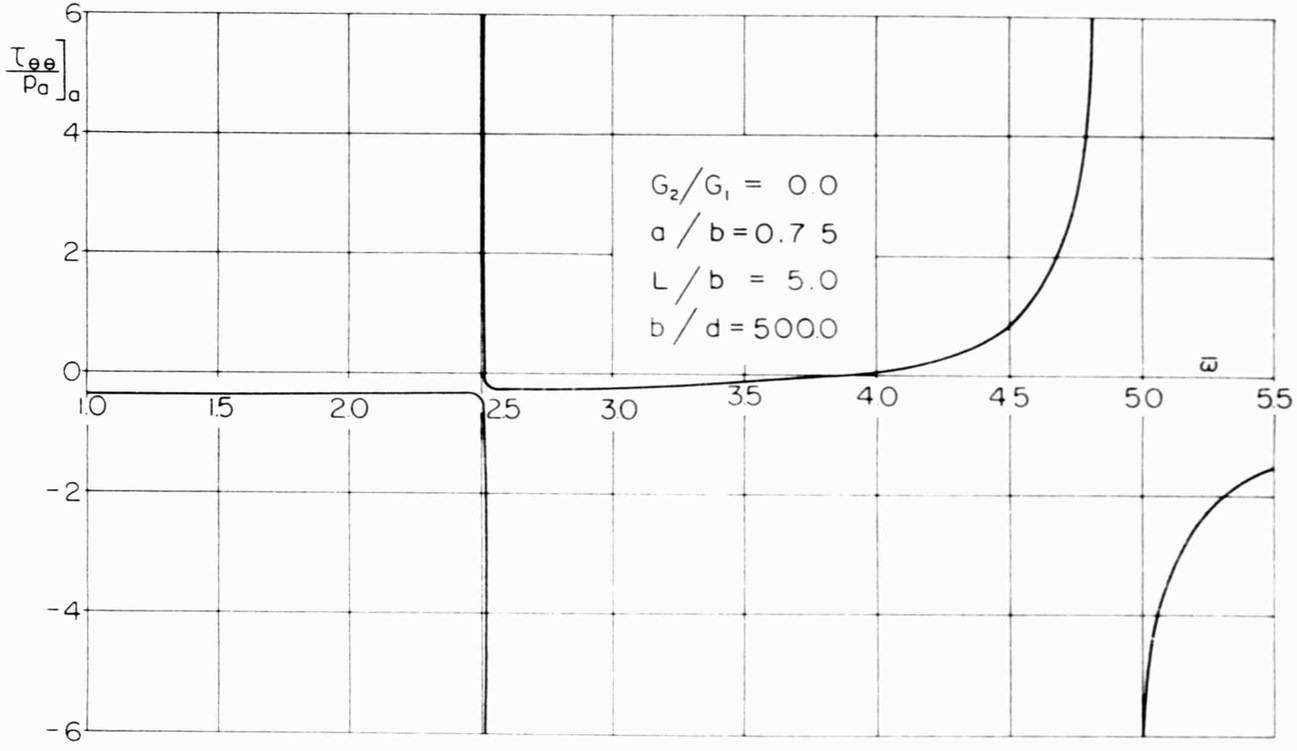

Figure 16a Circumferential Stress at the Bore for the Elastic Cylinder and Shell and Parameters as Indicated

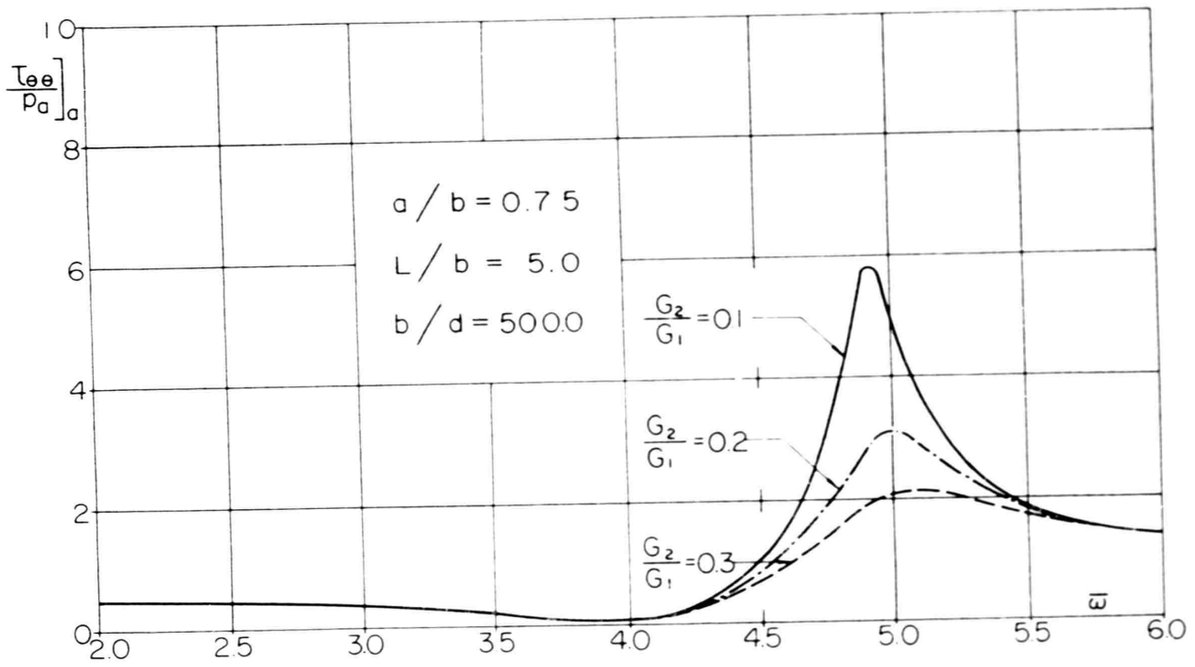

Figure 16b Absolute Value of Circumferential Stress at the Bore for Various Values of Damping and Parameters as Indicated

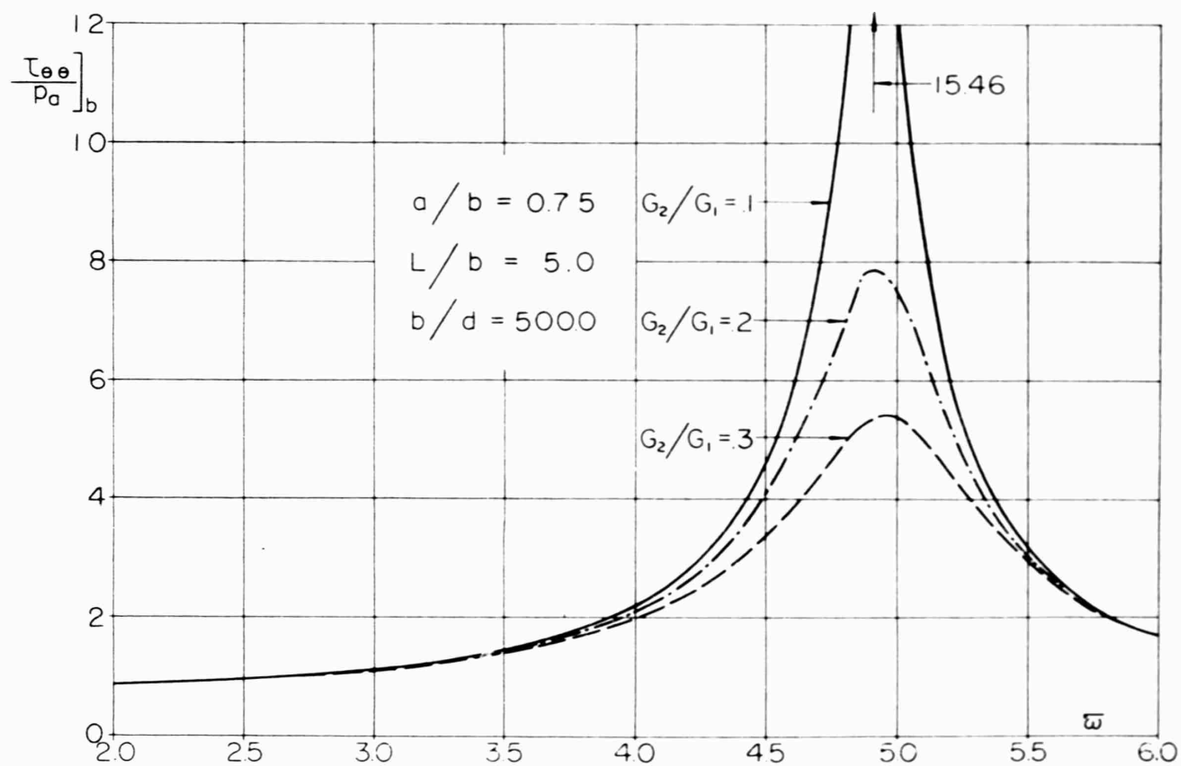

Figure 16c Absolute Value of Circumferential Stress at the Interface for Various Values of Damping and Parameters as Indicated

DISTRIBUTION LIST

ONR Solid Propellant Mechanics Reports

PART I - Members, POLARIS Committee

Office of Naval Research
Department of the Navy
Washington 25, D.C.
Attn: Dr. F. J. Weyl, Code 102

Applied Physics Laboratory
Johns Hopkins University
8621 Georgia Avenue
Silver Spring, Maryland
Attn: Dr. W. H. Avery

Naval Ordnance Laboratory
White Oak
Silver Spring, Maryland
Attn: Dr. D. F. Bleil

U.S. Naval Electronics Laboratory
San Diego 52, California
Attn: Dr. R. J. Christensen

Chief
Bureau of Ships
Department of the Navy
Washington 25, D.C.
Attn: Capt. W. H. Cross, Code 403

Woods Hole Oceanographic Institute
Woods Hole, Massachusetts
Attn: Dr. P. M. Fye

Chief
Bureau of Naval Weapons
Department of the Navy
Washington 25, D.C.
Attn: Dr. E. S. Lamar, CR-12

U.S. Naval Ordnance Test Station
China Lake, California
Attn: Dr. T. Phipps

Office of Naval Research
Department of the Navy
Washington 25, D.C.
Attn: Capt. W. T. Sawyer, Code 406

Chief, Bureau of Ships
Department of the Navy
Washington 25, D.C.
Attn: Dr. George Sponsler, Code 315

Director
Naval Reserach Laboratory
Department of the Navy
Washington 25, D.C.
Attn: Mr. P. Waterman, Code 5360

Missile and Space Division
Lockheed Aircraft Corporation
Palo Alto, California
Attn: Dr. W. F. Whitmore

Special Projects Office SP-114
Bureau of Naval Weapons
Department of the Navy
Washington 25, D.C.
Attn: LCDR R. H. Yerbury
Executive Secretary

PART II - Members, SPIA Physical Properties Panel

Commander
Air Force Flight Test Center
Edwards Air Force Base, California
Attn: FTRS, D. Hart

Aberdeen Proving Group
Ballistic Research Laboratories
Aberdeen, Maryland
Attn: A. S. Elder
H. P. Gay

Redstone Arsenal
Army Rocket and Guided Missile Agency
Huntsville, Alabama
Attn: T. H. Duerr

Department of the Navy
Bureau of Naval Weapons
Washington 25, D.C.
Attn: RMMP-22, W. A. Bernett

U.S. Naval Ordnance Test Station
China Lake, California
Attn: K. H. Bischel
A. Adlcoff

U.S. Naval Propellant Plant
Indian Head, Maryland
Attn: W. J. Marciniak

Aerojet-General Corporation
P.O. Box 296
Azusa, California
Attn: K. H. Sweeny
K. W. Bills

Aerojet-General Corporation
P.O. Box 1168
Sacramento, California
Attn: J. H. Wiegand

Atlantic Research Corporation
Shirley Highway & Edsall Road
Alexandria, Virginia
Attn: M. G. DeFries

California Institute of Technology
Pasadena, California
Attn: J. P. Blatz
M. L. Williams

E. I. duPont de Nemours & Co.
Gibbstown, New Jersey
Attn: R. D. Spangler

Grand Central Rocket Company
P.O. Box 111
Redlands, California
Attn: E. Fitzgerald

Hercules Powder Company
Allegany Ballistic Laboratory
Cumberland, Maryland
Attn: J. H. Thacher

Hercules Powder Company
Bacchus Works
Magna, Utah
Attn: D. E. Nicholson

Jet Propulsion Laboratory
4800 Oak Grove Drive
Pasadena 3, California
Attn: R. F. Landel

Rocketdyne
Solid Propulsion Operations
P.O. Box 548
McGregor, Texas
Attn: S. C. Britton

Rohm and Haas Company
Redstone Arsenal Research Division
Huntsville, Alabama
Attn: A. J. Ignatowski

Space Technology Laboratory. Inc.
5730 Arbor-Vitae Street
Los Angeles 45, California
Attn: W. G. Gottenberg

Stanford Research Institute
Menlo Park, California
Attn: Dr. T. L. Smith

Thiokol Chemicals Corporation
Redstone Division
Huntsville, Alabama
Attn: M. H. Cooper

United Technology Corporation
P.O. Box 358
Sunnyvale, California
Attn: Dr. Iwanciow
Dr. F. Lavacot

Solid Propellant Information Agency
APL/JHU, 8621 Georgia Avenue
Silver Spring, Maryland
Attn: M. T. Lyons (3)

PART III - Activities and Contractors - Concerned with Propellant Mechanics

Government

Chief of Naval Research
Department of the Navy
Washington 25, D. C.
Attn: Code 439 (3)
Code 411
Commanding Officer
Cognizant CNR Branch Office

Armed Services Technical
Information Agency
Arlington Hall Station
Arlington 12, Virginia (10)

Office of Technical Services
Department of Commerce
Washington 25, D.C.

Director of Defense Research and
Engineering
The Pentagon
Washington 25, D.C.
Attn: Technical Library

Advanced Research Projects Agency
Defense Research and Engineering
The Pentagon
Washington 25, D.C.
Attn: A.M. Rubenstein

Director, Special Projects
Department of the Navy
Washington 25, D.C.
Attn: SP001 (Dr. J. P. Craven)
SP271 (LCDR R. L. McArthy)

Chief, Bureau of Naval Weapons
Department of the Navy
Washington 25, D.C.
Attn: RRRE-6 (Dr. C. Boyars)
RMMP-2 (Dr. O. H. Johnson)
RMMP-11 (Mr. I. Silver)

Commander
Air Force Flight Test Center
Edwards Air Force Base, California
Attn: FTRS

Commander
Ogden Air Material Area
Hill Air Force Base, Utah
Attn: OOMQCC, H. A. Matis

Commander
Air Force Office of Scientific Research
Washington 25, D.C.
Attn: Mechanics Division

Commanding General
Aberdeen Proving Ground
Maryland
Attn: Ballistic Research Labs.
ORDBG-BLI

Commander
Army Rocket and Guided Missile Agency
Redstone Arsenal, Alabama
Attn: Technical Library
ORDXR-OTL
ORDAB-HSI

Department of the Army
Office, Chief of Ordnance
Washington 25, D.C.
Attn: ORDTB, J. A. Chalmers

Director
Plastics Tech. Eval. Center
Picatinny Arsenal
Dover, New Jersey

U.S. Army Research Office
2127 Myrtle Drive
Duke Station
Durham, North Carolina
Attn: Div. of Engineering Sciences

Chief of Naval Operations
Department of the Navy
Washington 25, D.C.
Attn: Op 07T
Op 03EG

Quality Evaluation Laboratory
Naval Ammunition Depot
Concord, California
Attn: D. R. Smathers

U.S. Naval Ordnance Laboratory
Non Metallic Materials Division
Silver Spring, Maryland
Attn: H. A. Perry, Jr.

U.S. Naval Ordnance Test Station
China Lake, California
Attn: J. T. Bartling

U.S. Naval Propellant Plant
Indian Head, Maryland
Attn: J. Browning
L. Papier (L)

Office of Naval Research
Branch Office
495 Summer Street
Boston 10, Massachusetts
Attn: Dr. J. H. Faull, Jr.

National Aeronautics & Space Adm.
1570 H Street, N.W.
Washington 25, D.C.
Attn: Chief, Div. of Research
Information

Contractors

Atlantic Research, Inc.
Shirley Highway & Edsall Road
Alexandria, Virginia
Attn: M. G. DeFries

Battelle Memorial Institute
505 King Avenue
Columbus 1, Ohio
Attn: J. Harry Jackson

Brown University
Division of Applied Mathematics
Providence 12, Rhode Island
Attn: Prof. E. H. Lee
Prof. R. S. Rivlin

University of California
College of Engineering
Berkely 4, California
Attn: Prof. Paul M. Naghdi

Catholic University of America
Department of Civil Engineering
620 Michigan Avenue, N.E.
Washington, D.C.
Attn: Prof. A. J. Durelli

Columbia University
Department of Civil Engineering
Amsterdam Avenue & 120th Street
New York 27, New York
Attn: Prof. A. M. Freudenthal

Materials Technology, Inc.
11 Leon Street
Boston 15, Massachusetts
Attn: Dr. R. G. Cheatham

New York University
Depart. of Aeronautical Engineering
University Heights
New York 53, New York
Attn: Prof. H. Becker

University of Pennsylvania
Graduate Division of Engineering Mechanics
Philadelphia 4, Pennsylvania
Attn: Prof. Z. Hashin

Polytechnic Institute of Brooklyn
333 Jay Street
Brooklyn 1, New York
Attn: Prof. F. Romano
Prof. J. Klosner
Prof. F. Ullman

Southwest Reseatch Institute
8500 Culebra Road
San Antonio 6, Texas
Attn: Dr. R. C. DeHart

Central Laboratory T. N. O.
134 Julianalaan
Delft, Holland
Attn: Dr. F. Schwarzl

Aerojet-General Corporation
Solid Rocket Plant
Sacramento, California
Attn: Dr. W. O. Wetmore (2)

Aerojet-General Corporation
P.O. Box 1168
Sacramento, California
Attn: A. Fraser
Dr. Zickel

Amcel Propulsion, Inc.
Box 3049
Asheville, North Carolina
Attn: R. N. Lowrey

American Cyanamid Company
1937 West Main Street
Stamford, Connecticut
Attn: Dr. V. Wystrach

Chief, Bureau of Ships
Department of the Navy
Washington 25, D. C.
Attn: Code 335

Professor R. L. Bisplinghoff
Department of Aeronautical Engineering
Massachusetts Institute of Technology
Cambridge 39, Massachusetts

Chief, Bureau of Yards & Docks
Department of the Navy
Washington 25, D. C.
Attn: Code 70

Commanding Officer & Director
David Taylor Model Basin
Washington 7, D. C.
Attn: Code 700

Director
Materials Laboratory
New York Naval Shipyard
Brooklyn 1, New York

Officer-in-Charge
Naval Civil Engineering Research
and Evaluation Laboratory
U.S. Naval Construction Battalion
Center
Port Hueneme, California

Commander
U.S. Naval Proving Ground
Dahlgren, Virginia

Commanding Officer & Director
U.S. Naval Engineering Experiment
Station
Annapolis, Maryland

Superintendent
U. S. Naval Postgraduate School
Monterey, California

National Sciences Foundation
1520 H Street, N.W.
Washington, D. C.
Attn: Engineering Sci. Div.

Professor H. H. Bleich
Department of Civil Engineering
Columbia University
Amsterdam Avenue & 120th Street
New York 27, New York

Professor B. A. Boley
Department of Civil Engineering
Columbia University
Amsterdam Avenue & 120th Street
New York 27, New York

Professor B. Budiansky
Department of Mechanical Engineering
School of Applied Sciences
Harvard University
Cambridge 38, Massachusetts

Professor G. F. Carrier
Pierce Hall
Harvard University
Cambridge 38, Massachusetts

Professor D. C. Drucker
Division of Engineering
Brown University
Providence 12, Rhode Island

Professor J. Ericksen
Mechanical Engineering Department
Johns Hopkins University
Baltimore 18, Maryland

Professor A. C. Eringen
Department of Aeronautical Engineering
Purdue University
Lafayette, Indiana

Mr. Martin Goland, President
Southwest Research Institute
8500 Culebra Road
San Antonio 6, Texas

Professor J. N. Goodier
Department of Mechanical Engineering
Stanford University
Stanford, California

University of California
Berkely, California
Attn: Dr. K. S. Pister

Catholic University of America
Department of Civil Engineering
Washington, D.C.
Attn: J. Baltrukonis

University of Florida
College of Engineering
Gainseville, Florida
Attn: J. Griffith

University of Illinois
Department of Aero Engineering
Urbana, Illinois
Attn: Dr. H. H. Hilton

E. I. duPont de Nemours and Co.
Gibbstown. New Jersey
Attn: R. D. Spangler

Grand Central Rocket Company
P.O. Box 111
Redlands, California
Attn: A. T. Camp

Hercules Powder Company
Allegany Ballistics Laboratory
Cumberland, Maryland
Attn: Dr. R. Steieberger (2)

Jet Propulsion Laboratory
4800 Oak Grove Drive
Pasadena 3, California
Attn: G. Lewis

Lockheed Missile & Space Company
1122 Jagels Road
Sunnyvale, California
Attn: E. Luken (2)

North American Aviation
Rocketdyne Division
6633 Canoga Avenue
Canoga Park, California
Attn: F. Cramer

Rohm & Haas Company
Redstone Arsenal Research Division
Huntsville, Alabama
Attn: H. Shuey

Thiokol Chemical Corporation
Redstone Division
Huntsville, Alabama
Attn: Technical Director
J. Wise

PART IV - Activities and contractor concerned with other aspects of Elastomer Mechanics

Government

Commanding Officer
Office of Naval Research
Branch Office
John Crerar Library Building
86 E. Randolph Street
Chicago 11, Illinois

Commanding Officer
Office of Naval Research
Branch Office
346 Broadway
New York 13, New York

Commanding Officer
Office of Naval Research
Branch Office
1030 E. Green Street
Pasadena, California

Commanding Officer
Office of Naval Research
Branch Office
1000 Geary Street
San Francisco, California

Commanding Officer
Office of Naval Research
Branch Office
Navy 100, Fleet Post Office
Box 39 FPO
New York, New York (5)

Director
Naval Research Laboratory
Washington 25, D.C.
Attn: Tech. Info. Officer (6)
Code 6200
Code 6210

Professor P. G. Hodge
Department of Mechanics
Illinois Institute of Technology
Chicago 16, Illinois

Professor N. J. Hoff, Head
Division of Aeronautical Engineering
Stanford University
Stanford, California

Professor J. Kempner
Dept. of Aeronautical Engineering
and Applied Mechanics
Polytechnic Institute of Brooklyn
333 Jay Street
Brooklyn, New York

Professor R. D. Mindlin
Dept. of Civil Engineering
Columbia University
Amsterdam Avenue & 120 Street
New York 27, New York

Professor William A. Nash
Dept. of Engineering Mechanics
University of Florida
Gainesville, Florida

Professor N. M. Newmark, Head
Dept. of Civil Engineering
University of Illinois
Urbana, Illinois

Professor E. Reiss
Institute of Mathematical Sciences
New York University
25 Waverly Place
New York 3, New York

Professor W. Prager, Chairman
Physical Sciences Council
Brown University
Providence 12, Rhode Island

Professor E. Reissner
Dept. of Mathematics
Massachusetts Institute of Technology
Cambridge 39, Massachusetts

Professor Bernard W. Shaffer
Dept. of Mechanical Engineering
New York University
University Heights
New York 53, New York

Professor Eli Sternberg
Dept. of Mechanics
Brown University
Providence 12, Rhode Island

Professor A. S. Velestos
Dept. of Civil Engineering
University of Illinois
Urbana, Illinois